Koninklijk Meteorologisch Instituut van België

Institut Royal Météorologique de Belgique

Royal Meteorological Institute of Belgium

RMI

On the Science of Lightning:
An Overview

dr. Dieter R. Poelman

2010

On the Science of Lightning:
An Overview
dr. Dieter R. Poelman

Scientific committee:
dr. ir. Steven Dewitte
dr. ir. Laurent Delobbe
dr. Fabian Debal

Contents

Abstract

This manuscript aims at summarising the different physical properties involved in lightning discharges in thunderclouds. As well as to present the different techniques to observe the electromagnetic characteristics emitted by the lightning discharge, a concise overview is given of the different European networks committed to lightning observations. Finally, we outline various scientific studies that can be executed with the observed lightning properties. As such, we hope to provide the reader with a brief understanding of the different aspects associated with lightning studies. We conclude with some future prospects of the lightning studies at the Royal Meteorological Institute of Belgium (RMI).

1   Introduction

Extreme weather phenomena have always been one of humans profound interests and fascinations. This is apparent in the different mythologies impersonating the God of Thunder and Weather from the time in ancient Egypt (Typhon), China (Tien Mu) and India (Indra) to the ancient Greek times of which Zeus, whose symbol is a lightning flash, is the most famous one. As such, lightning must have been known by many civilisations throughout the history of mankind. Furthermore, fossil evidence (Harland & Hacker 1966) confirms that terrestrial lightning has been present for over 250 million years. Thus, electrification is a long-lived phenomenon, whose abundance and longevity has even let to the suggestion that lightning lies at the formation of molecules giving rise to life (Miller 1953).

In this chapter we give a brief historical overview of the pioneering studies of the electrical nature of the atmosphere (Section 1.1) and discuss the global electric circuit that is thought to be energized by thunderstorms (Section 1.2). In Sect. 1.3 current theories on cloud electrification are discussed.

1.1   Historical overview

The first experimental studies of the electrical characteristics of the Earth's atmosphere date back to the mid-18$^{\text{th}}$ century where, in Marly-la-Ville near Paris, experiments with an iron rod provided the first direct proof that thunderclouds contain electricity. These tests were a direct result from Benjamin Franklin's published letters on electricity in which he designed experiments to test the hypotheses that thunderstorms somehow generate electricity. This was shortly afterwards followed by Franklin himself (and others) who drew sparks from a moist string of a kite. It is worth noting that in addition to showing that clouds contain electricity further pioneering experiments of Franklin proved that the lower part of a thunderstorm is generally negatively charged (Franklin 1774). Shortly after the experiment at Marly that confirmed the electrical nature of thunderstorms, Lemonnier (1752) discovered electrification in fair weather. During subsequent years, many other scientists conducted experiments studying the atmospheric electricity. From this it was further established that the Earth's surface is charged negatively and the air positively, with an associated vertical electric field in fair weather being about $100\,\text{Vm}^{-1}$. This has let to the concept of a global electric circuit (GEC), first suggested by Wilson (1920, 1929), in which the electric field and current flowing in the lower atmosphere, ionosphere and magnetosphere were linked together for the first time. In the twentieth century, balloon findings provided additional data on the vertical profiles of atmospheric electrical parameters, generally finding a decrease in the vertical electric field's magnitude with height (Chauveau 1925; Chalmers 1967). In addition, pioneering measurements of the electrical conductivity, finding an increase with altitude, contributed to the knowledge of the fair weather atmospheric electricity we know today. As such, the fundamental basis to understand the atmospheric electrical circuit, and consequently the electric nature of clouds, was written down. Today current studies still reap the fruits of this pioneering work.
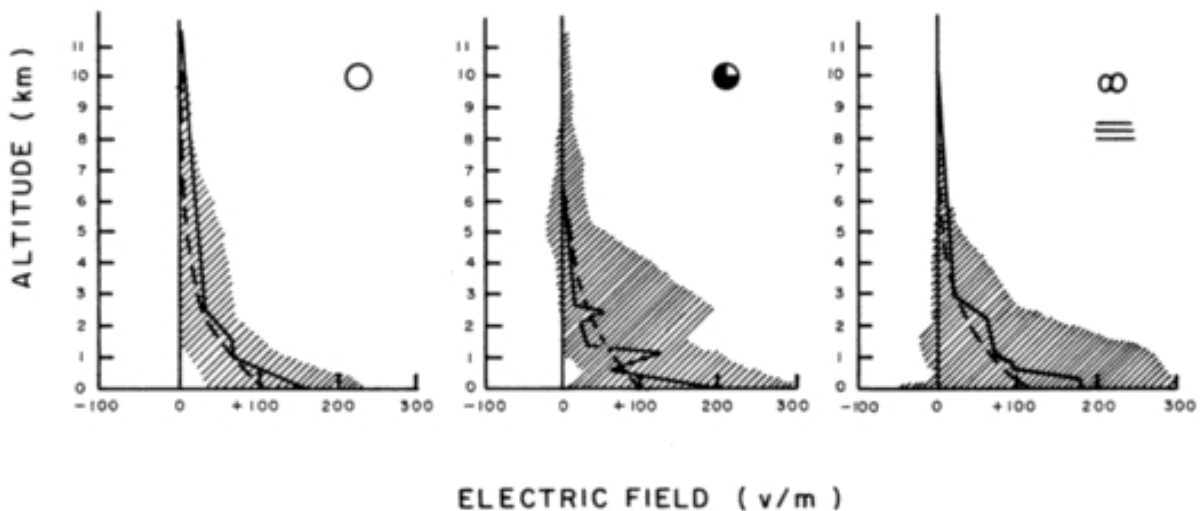
Figure 1: The atmospheric electric field versus altitude in the lower atmosphere during fair weather (*left*), cloudiness without precipitation (*middle*), and during haze and fog (*right*). The black curves show typical measurements and the shaded areas show the spread of the values (Fischer 1977).

1.2   Fair-weather system & the global electric circuit

The Earth is bombarded by a vast amount of energetic solar and galactic cosmic ray particles creating ions in our atmosphere. Below 50 km the atmosphere is conducting owing to these 'cosmic ray ions' and the natural radioactivity of the Earth, the latter having an effect from the ground level up to a height of $\sim$3 km. Free electrons at these heights are short-lived, as they recombine with the numerous neutrals on time scales on the order of microseconds. Therefore, the contribution of free electrons to the conductivity below 50 km can be neglected. However, with increasing height become electrons the major contributor to the atmospheric conductivity. On average, the electrical conductivity at sea level is on the order of 10^{-14} Sm^{-1}, increases rapidly with height to about 10^{-11} Sm^{-1} at 35 km and is altered to 10^{-3} Sm^{-1} at 100 km, comparable to the value of the conductivity level of the Earth's surface. It is usually assumed that the atmosphere above a height of about 60 km becomes conductive enough to consider it as an equipotential region, owing to the abrupt increase in free electrons at these heights. This region, where free electrons are the major contributor to the conductivity is sometimes referred to as the *electrosphere*. A consequence of the increase in conductivity with altitude is that the columnar resistance of the atmosphere is concentrated near the surface. On the other hand, the electric field – measured between the ionosphere and the Earth – is about 100 Vm^{-1}, drops rapidly with height to about 300 mVm^{-1} at 30 km at mid-latitudes (Gringel et al. 1986) and to 1 μVm^{-1} or so at about 85 km (Reid 1986). This results, after evaluation of the line integral of the electric field intensity from the Earth's surface to the height of the electrosphere, in an ionospheric potential of approximately 300 kV. The behavior of the electric field strength as a function of height in the lower atmosphere is illustrated in Fig. 1. The variations of different profiles, shown by the hachured areas, are mainly caused by conductivity variations, especially in the lower troposphere, rather than by variations of the ionospheric potential itself. Notice that the scatter is greatly increased during periods of cloudiness and haze or fog, whereas the mean profile still shows a pattern typical for fair-weather conditions. During rain and snow and especially in thunderclouds, the scatter in the field values becomes much larger, including regions with large negative field values. These large variations of the electric field strength are caused by regions of high-space-charge density of both signs in these clouds.

Since air in the lower atmosphere is not a perfect isolator, there is a vertical current flow from the positively charged ionosphere to the Earth's surface. This current has been measured to be on average about 2.7 μA/km^2 and is called the *fair-weather current*. Integrating over the Earth's surface, this results in a current of $\sim$1500 A. Since measurements have never shown a complete absence of this fair-weather electric field for any length of time, there must be a
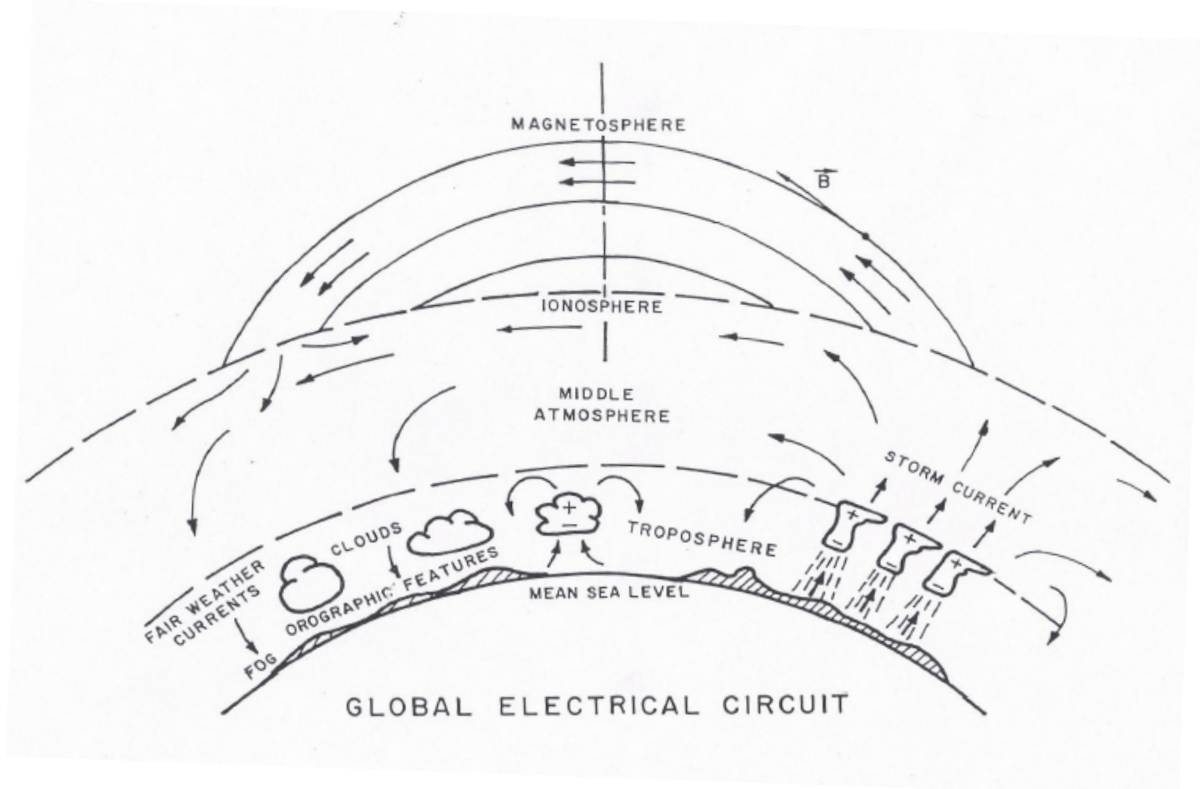
Figure 2: Schematic diagram of various electrical processes in the global electric circuit (GEC). Vector $\vec{B}$ shows the direction of the Earth's geomagnetic field, and arrows show the direction of the current flow in the regions of the tropospheric, ionospheric and magnetospheric generators (Siingh et al. 2007).

mechanism to replenish the lost charge back to the ionosphere. Otherwise, this fair-weather current would neutralise the charge on Earth and in the atmosphere on a time scale on the order of 10 minutes, depending on the amount of pollution in the air. It was suggested by Wilson (1920) that the negative charge on Earth is maintained by the action of thunderstorms. At any time, there are on average about 1500 active thunderstorms across the world. Hence, the total current flowing from the cloud tops to the ionosphere is roughly 1 A per thunderstorm (Gish & Wait 1950). Negative charge is brought to the Earth mainly by lightning discharges (most of which transport negative charge to the ground). This has been measured to be on average consistent with an upward current[1] of $0.6\,\mu\text{A/km}^2$. The net precipitation current is thought to transport positive charge to ground, consistent with a downward current of $0.9\,\mu\text{A/km}^2$. Positive charge is also transported upwards via point sources (e.g., high buildings) at a rate of about $3.0\,\mu\text{A/km}^2$. As a result, a net positive current of $2.7\,\mu\text{A/km}^2$ is directed upwards. To replenish the charge the ionosphere is losing via the fair-weather current, the latter upward directed current flows from the top of the thunderstorm to the ionosphere, also known as the *Wilson current*. Besides the vertical flow of current in the lower atmosphere, horizontal current flows freely along the highly conducting Earth's surface and in the ionosphere. This, in its turn is closed by the current flowing from the ground into the thunderstorm and from the top of the thunderstorm to the ionosphere and back from the ionosphere to the ground through the global fair-weather flow. This global electric circuit concept (GEC) is illustrated in Fig. 2. The horizontal current spreads around the globe through the ionosphere and magnetosphere along the geomagnetic field lines to the opposite hemisphere. As mentioned above, the main source of electric fields in the troposphere are thunderstorms. However, in the ionosphere there must be another source providing electric fields. This is established by the convective flow resulting from the Sun's heating

---

[1]According to the physics sign convention a downward directed field is negative because it is in the direction opposite to that of the radial coordinate vector of the spherical system whose origin is at the Earth's center. A positive current is induced by an upward-directed field, which is defined as positive.

influence in the upper regions of the atmosphere, leading to tidal winds driving the ionospheric plasma. Ions and electrons are affected differently by these winds as a result of the difference in mass. Ions are massive particles and move with the neutrals, while the geomagnetic field controls the motion of the electrons at these heights. As a result, these tides generate horizontal potential differences on the order of 5–15 kV within the ionosphere. In the magnetosphere, on the other hand, the horizontal current flow is generated by the solar wind. This results in a drift motion causing horizontal charge separation of the order 40–100 kV across the magnetic conjugate polar cap. Note that the GEC is not constant at all time since any variation in the solar wind parameters lead to a modification of the stratosphere and troposphere and hence results in the modulation of the current density in the global atmospheric electric circuit from the ionosphere to the Earth.

1.3   Electrical structure of lightning-producing clouds

The classification of clouds was introduced by Luke Howard in 1802, a British pharmacist. His classification scheme is still used to date, with minor changes to it. It makes use of the Latin words 'cirrus', 'stratus', 'cumulus' and 'nimbus' which respectively mean 'curl of hair', 'layer', 'heap' and 'rain'. In general, all clouds can be divided into four main classes of groups. The identification of the first three groups is based on the height of the cloud base above the ground. These groups are (1) low-level clouds (cloud base from 0 to 2 km) consisting out of the stratus, stratocumulus and nimbostratus cloud, (2) mid-level clouds (cloud base from 2 to 6 km) such as the altocumulus and altostratus, and finally (3) high-level clouds (cloud base from 6 to 13 km) containing the cirrocumulus, cirrostratus, cirrus. The fourth group includes vertically developed clouds like the cumulonimbus and cumulus. Note that each of these cloud types can be further divided into different variants. The giant under these types is the cumulonimbus, and is the primary source of lightning. However, not every cumulonimbus produces lightning (see Sect. 5.1). Therefore, thunderclouds can be called lightning-producing cumulonimbus clouds.

Clouds are formed when parcels of air cool down below the dew point. This depends on the relative humidity in the parcel. When the saturation point is exceeded, moisture condenses on airborne particles, to form the many small water particles that constitute the visible cloud. It is worth mentioning that these airborne particles, or cloud condensation nuclei, are ultra-fine aerosols resulting mainly from the ionisation produced by cosmic rays in the troposphere and stratosphere. In the atmosphere the air can cool in three ways: (i) by rising and expanding, (ii) via contact with a cooler surface, or (iii) through evaporative cooling[2]. Processes that lead to the rise of air parcels include (i) convection, in which air parcels are heated above a warm surface, (ii) forced rising due to the presence of hills or mountains (called orographic rise) and (iii) rising due to meteorological perturbation forcing, e.g., fronts, through, ...

Consider now a parcel of warm, moist air. This will rise and cool by adiabatic expansion, i.e., without loss of heat or mass across the boundaries of the parcel, and will continue to do so until the temperature of the parcel becomes equal or less then the air temperature surrounding it. As it rises, its relative humidity[3] will increase, while its specific humidity remains[4] constant. Since the saturation vapor pressure decreases almost exponentially with decreasing temperature, it will start to condensate. The height above which this happens is called the *lifting condensation level* (LCL). In the troposphere, the temperature decreases with increasing height at a rate of about 1°C per 100 m. As a result, when a parcel rises above the 0°C isotherm at a height higher than the LCL some water particles will freeze, while others remain liquid at temperatures colder than 0°C, called supercooled particles. It has been found that at temperatures below -40°C all particles will be frozen. It is in this temperature regime, between 0°C and -40°C that most electrification, i.e., charge transfer and separation, of thunderclouds takes place due to the co-existence of liquid water and ice particles. Here, we shortly sketch the different mechanisms that lie at the basis of cloud electrification and lead to the typically observed *tripole* structure

---

[2]Evaporative cooling is a physical phenomenon in which evaporation of a liquid, typically into surrounding air, cools an object or a liquid in contact with it. By evaporating, the most energetic molecules escape and take their share of heat with them. The liquid has thus lost energy and becomes cooler.

[3]Relative humidity describes the amount of water vapor that exist in a gaseous mixture of air and water vapor.

[4]Specific humidity is the ratio of water vapor to air *in a particular mass*.
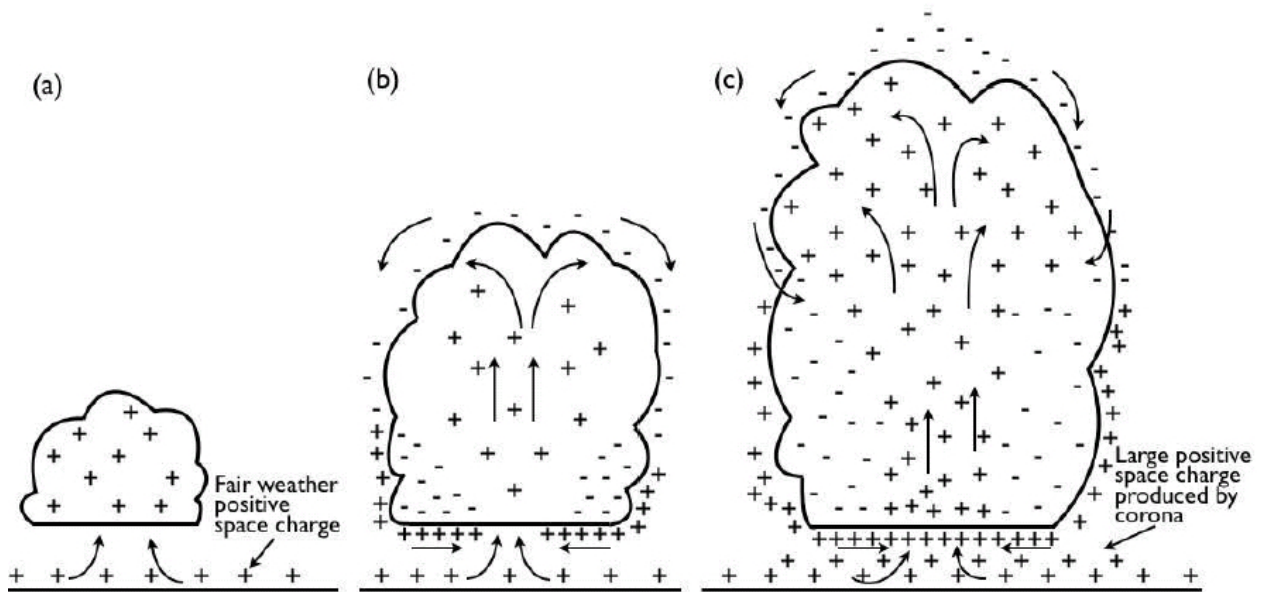
Figure 3: Illustration of the convection mechanism of cloud electrification. (a) Positive space charge is ingested into the cloud. (b) A negative screening layer, consisting out of electrons and negative ions, forms on the cloud particles on the outside boundary, which moves down the sides toward the cloud base. Additional positive charge is further ingested at the base, and further negative charge flows to the upper cloud boundary to replace the loss of the screening layer that flowed to the cloud base along the sides. (c) The lower accumulation of negative charge increases the electric field strength to a magnitude large enough to generate positive corona from ground objects. The corona becomes an additional source of positive charge that feeds into the cloud. Adapted from MacGorman and Rust (1998).

in thunderstorms, i.e., a net positive charge near the top, a net negative charge below it and an additional smaller positive charge at the bottom of the cloud. For a thorough description of the current hypotheses for charge-separation mechanisms in thunderstorms, we refer the interested reader to MacGorman and Rust (1998). Here, we discuss two main routes to electrify a cloud, i.e., through inductive and/or via non-inductive processes:

(1) *Inductive charging*: refers to processes that are induced by the presence of an electric field. The existence of a fair-weather field ensures that water particles suspended in the atmosphere will become polarized. In a vertical, downward directed field (conventionally defined to be negative), such polarization will cause an excess of positive charge to accumulate in the lower part of the particle, while negative charge will be preferably located in the upper part. While the particle drops it will meet negatively and positively charged particles. Since the lower part is positively charged, negatively charged particles are attracted by the falling droplet, while positively charged particles are pushed away. As a result, the particle grows and becomes more negatively charged. This leads to a cloud with positively charged particles at the upper part, and negatively charged particles at the bottom. However, the present consensus in the literature judges inductive processes to have little importance in the early stages of cloud electrification and to be of secondary importance in later stages, when the intensity in the in-cloud electric field becomes much stronger than the fair-weather field.

(2) *Non-inductive charging*: refers to those charging processes which are indifferent to the presence of an external electric field, and whose efficiency is not impacted by its strength. The two main mechanisms are:

(i) *Convection mechanism*: Here, the sources of positive and negative charges are considered to be external, i.e., via fair-weather space charge, natural radioactivity near the land surface and cosmic rays near the cloud top. The positive charges near ground are carried via warm
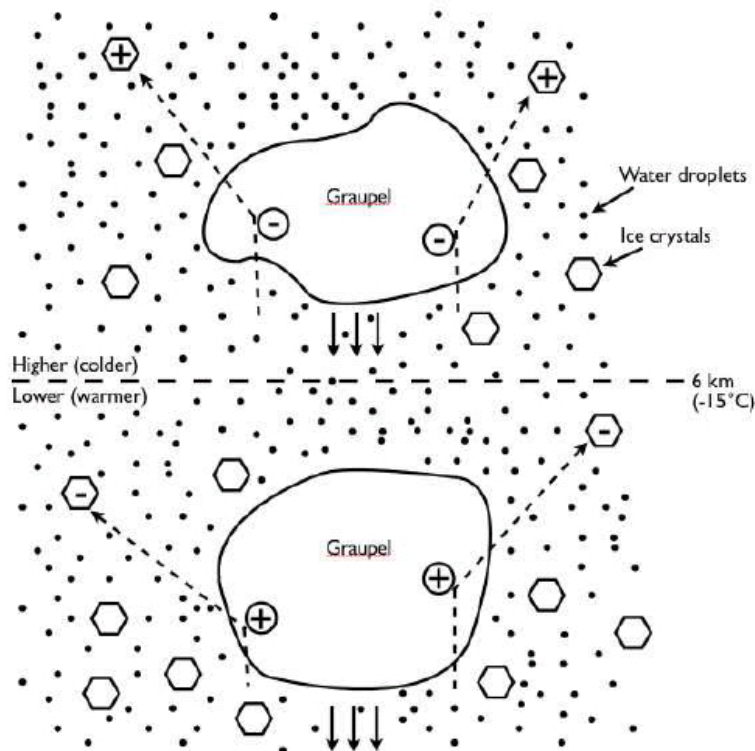
5

Figure 4: Charge transfer by collisions in the graupel-ice mechanism of cloud electrification. Here, it is assumed that the reversal temperature T_R is -15°C at a height of 6 km.

air updrafts to the top of the growing cumulus. As a result, negative charge – produced by the cosmic rays at the top of the cloud – are attracted and attached to the cloud's boundary. Subsequent cooling and convective circulation result in a downdraft and are assumed to carry the negative charge down the side of the cloud towards the cloud's base. This, in its turn, serves to produce a positive corona near the Earth's surface, which leads to an additional positive charge under the cloud. A schematic representation of this mechanism is plotted in Fig. 3. It has been found that the amount of corona charge transported from the Earth's surface to the bottom of the cloud during the lifetime of a thunderstorm is comparable to the charge involved in a single lightning (Chauzy & Soula 1999). Hence, the convection mechanism tends not to be responsible for the overall observed cloud electrification, since a thunderstorm generally produces several lightning discharges during its lifetime.

(ii) *Graupel-ice mechanism*: The basic description of this process calls for collisions between graupel[5] and small cloud-ice particles. Fig. 4 shows a schematic representation of this mechanism. Laboratory experiments (e.g., Jayaratne et al. 1983) found that there is a certain temperature, called the reversal temperature T_R, above which graupel particles acquire positive charge and, vice versa, acquire negative charge when the temperature falls below T_R. As a result, the smaller ice crystals become charged positively and then carried to the upper regions, while the larger graupel particles charge negatively and descend relative to the smaller particles after collision. Thus, the charge transfers during encounters of ice crystals and graupel will lead to the normal polarity usually found in the observations of terrestrial clouds. Note that observations of thunderclouds show a typical *tripolar* structure, i.e., with an additional

---

[5]Solid precipitation is subdivided by density and fall speed into *snow* (lowest density, with fall speeds of ≈0.3–1.5 ms^{-1}), *graupel* (intermediate density, with fall speeds of ≈1–3 ms^{-1}), and *hail* (greatest density with fall speeds up to 50 ms^{-1}). The density of graupel particles is less than that of hail, because much of graupel growth is by *riming*, a process in which accreted particles freeze rapidly to the graupel as distinct particles. When particles are collected fast enough so that latent heat of freezing warms the graupel to 0°C, liquid water coexist with ice and can fill the ice structure. When the liquid finally freezes, graupel becomes hail.
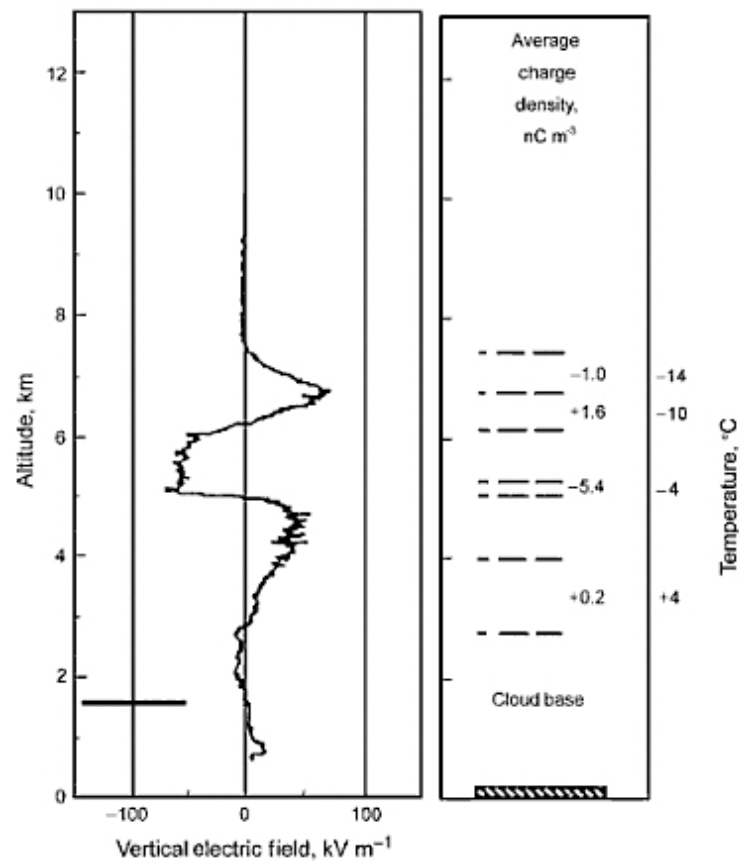
Figure 5: Balloon measurement of a vertical electric field inside a small thunderstorm. An upward-directed electric field is defined as positive. The values of the inferred average charge density are shown on the right (in nCm^{-3}; based on Gauss's law relating the distribution of electric charge to the electric field). The profile is indicative of a 'classical' tripole with an upward negative screening layer. Adapted from Marshall & Rust (1991).

small positively charge region at the bottom of the cloud. The origin of these lower positive charges is speculative. It has been suggested to be deposited by lightning in the lower part of the cloud by Marchall and Winn (1982). Besides this, Malan (1952) suggested that the lower positive charge center contains the charge that is produced by corona at ground and is subsequently carried into the cloud by conduction or convection.

Current electrification models strongly support the theory that graupel production in the layer from -10°C to -20°C is essential for the initial stages of lightning development (Zajac & Weaver 2002). This mechanism is considered to be the dominant electrification mechanism. Note that there are still major uncertainties about how many collisions actually occur in different regions of the cloud, what the collisional velocities are and the size of the crystals, etc. An example of data from balloon experiments by Marshall & Rust (1991) is presented in Fig. 5. These measurements indicate that, in addition to the three charge regions forming the 'classical' tripole model, there is a screening layer at the upper cloud boundary.

2   The lightning discharge

In Sect. 2.1 we focus on the first steps toward lightning initiation. Sect. 2.2 is devoted to the physics of downward negative lightning. Finally, we consider other types of lightning discharges in Sect. 2.3.

2.1   Lightning initation

Electrification and subsequent charge separation are prerequisites to develop an electric field within thunderclouds. In the same way as we experience a small electric discharge/shock when our hand approaches the doorhandle after acquiring some electric charge, the electric field between the positive/upper and negative/middle region in a thundercloud needs to be of some considerable strength in order to bridge the distance between the bottom of the cloud and the Earth's surface, i.e., in order for air to become a conductor. In short, a gas discharge is initiated when the electric field exceeds the threshold value necessary for a sufficient population of electrons to overcome collisional drag and accelerate to energies beyond the ionization potential. In addition, the ionization rate must exceed the net dissociative attachment[6] rate in order to have a net growth in the electron population. The field at which this occurs is the so-called electrical *breakdown field*. The value for the electrical field intensity for electric breakdown to occur at sea level in dry air is about $3 \times 10^6 \, \text{Vm}^{-1}$. With increasing height, this field value is reduced due to the decrease in air pressure. Consequently, at the height of the cloud, e.g., 6 km, the required field strength is roughly $1.6 \times 10^6 \, \text{Vm}^{-1}$. At present, such large field strengths have never been detected. The largest electric field magnitude typically observed at the cloud base is on the order of $5 \times 10^4 \, \text{Vm}^{-1}$, almost two orders of magnitude lower than the required critical value for break-down. This discrepancy has two possible explanations. The first says that stronger than observed electrical fields are present within thunderstorms. But these are confined to too small regions in order to be easily detected, owing to the small volume sizes of cloud regions containing the largest charges in active thunderstorms. However, this does not explain why such large highly compacted fields exist in the first place. Secondly, laboratory experiments demonstrated that the electric field needed to produce a discharge substantially reduces with the presence of ice crystals and hydrometeors[7]. However, even with this reduction the observed electric field strengths are too low to explain the occurrence of discharges in thunderstorms. Thus, a 'classic' discharge mechanism cannot explain the presence of lightning. But there exists another form of discharge, which is called the *runaway* breakdown. This was first introduced by Gurevich et al. (1992) and involves an avalanche of relativistic electrons that are collimated by the electric field to form an electron beam. In a conventional discharge, electrons move with relatively low speed, as they are hampered by the molecules in the air. However, experiments have shown that when electrons move with speeds of at least $6 \times 10^6 \, \text{m/s}$, the frictional force experienced by electrons decreases with increasing speed. As such, the electron gains more energy from the electric field between collisions with air particles than it loses in a collision. In a medium with a strong electric field Gurevich showed that it is possible to produce large amounts of highly energetic electrons from the ambient reservoir of low-energetic free electrons: runaway electrons produced in this way generate even more energetic electrons, achieved by powerful collisions with air molecules. These generated electrons, in their turn collide again with molecules creating even more energetic electrons, etc. This results in an avalanche of highly energetic electrons whose growth is exponential in time, since $\mathrm{d}n_e/\mathrm{d}t = \alpha_i n_e$. Thus, the production of electrons is proportional to the existing electron number density n_e and the ionisation rate coefficient α_i (Raizer 1997), and has as solution

$$n_e(t) = n_e(0) e^{\int_0^t \mathrm{d}t' \alpha_i(t')}. \tag{1}$$

---

[6]Dissociative attachment is a process in electron-molecule interactions. It is characterized by the interaction of the electron with the molecule resulting in an unstable negative ion and its subsequent dissociation into neutral and negative ion fragments before it could decay through the ejection of the extra electron.

[7]Hydrometeors are various liquid or frozen water particles. Hydrometeors whose motion is predominantly influenced by gravity (with fall speeds $\geq 0.3 \, \text{ms}^{-1}$) are called precipitation particles. All other hydrometeors are called cloud particles.
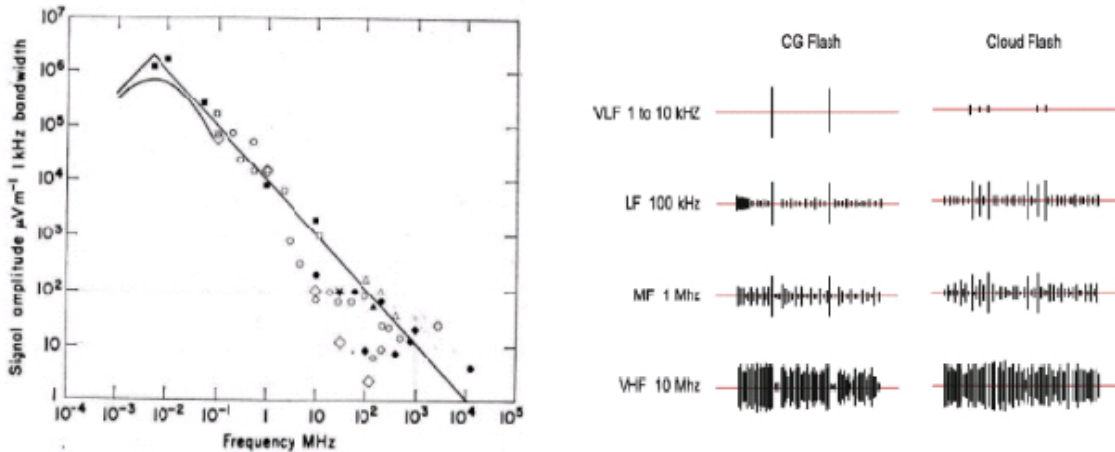
Figure 6: *Left*: The frequency spectrum of lightning according to Oetzel and Pierce (1969, reproduced in Chauzy et al. 2005). *Right*: Typical lightning radiation for a cloud-to-ground and a cloud flash. Adapted from Malan (1963).

This process can in principle be activated by one energetic electron. Therefore, cosmic ray interactions should be able to initiate the avalanche of energetic electrons, as these can penetrate to altitudes below the ionosphere. Note that the threshold electric field needed to initiate and continue the avalanche, the so-called breakeven electric field, is a factor of 10 below that for the conventional breakdown. The value for this breakeven field depends on altitude (air particle density) and initial electron energy. According to Suszcynsky et al. (1996), for electrons with energies of 200 keV, the breakeven field at an altitude of 10 km is $\sim 10^5$ Vm^{-1}. Macroscopic field strengths with values near and exceeding this threshold have been measured (e.g., Marshall et al. 2005; Stolzenburgh et al. 2007). As long as a strong electric field is present, this process will continue to grow. But can this theoretical model of runaway electrons be tested against observations? It is good to remember that a discharge due to runaway electrons will ionize a large amount of the surrounding air particles, producing highly energetic γ- and X-rays. Therefore, one way to test the hypotheses of runaway electrons is to look for large amounts of γ- and X-rays produced in lightning. The past several decades of research in this phenomenon has in fact seen an accumulation of evidence for the existence of this highly energetic radiation in direct association with many forms of the lightning discharge (McCarthy & Parks 1985; McCarthy & Parks 1992; Fishman et al. 1994; Eack et al. 1996; Moore et al. 2001; Dwyer 2003; Smith et al. 2005). In addition, studies have been performed linking the 11-year solar cyclus with the cosmic ray production. It was found that the cosmic ray intensity (CRI) shows 11-year temporal variations (Stozhkov et al. 2001) and, furthermore, that a growth (decay) of CRI leads to an enhancement (decrease) of lightning activity in thunderstorms (Stozhkov 2003; Ermakov & Stozhkov 2003).

2.2 Downward negative lightning discharge

In previous sections we have discussed the electrical nature of the atmosphere and more specific in thunderstorms with its typical tripolar structure, as well as the possible mechanisms that initiate the lightning discharge. In short, the local discharge between the main negative and lower positive region frees electrons in the negative region, previously immobilized by attachment to water or ice particles. Since the mass of electrons is very small, they are extremely mobile. Subsequently, they overrun the lower region in the thundercloud, neutralizing its small positive charge and continue their trip towards the ground. With this information at hand, we are now able to go into more detail into the physics of the processes that lie at the basis to form the lightning channel.

In general, two types of lightning occur within a thunderstorm, i.e., cloud discharges (CC) and cloud-to-ground lightning (CG). The first type are lightning discharges that do not involve
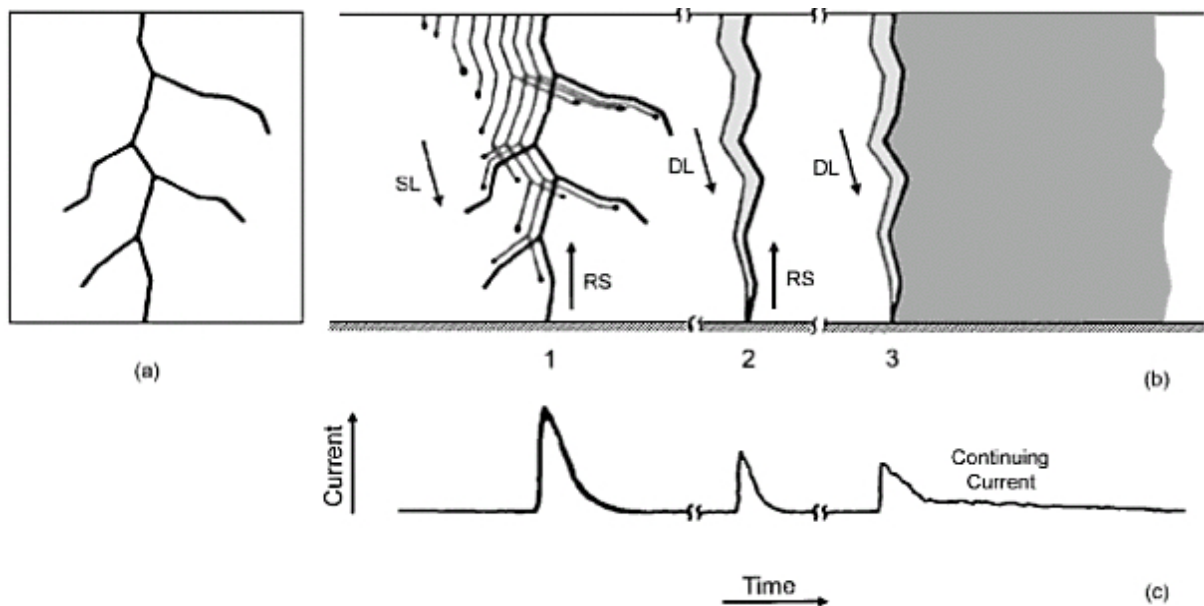
Figure 7: Schematic representation of the different steps associated with a downward three-stroke ground lightning flash and the corresponding current at the channel base: (a) still-camera image, (b) streak-camera image, and (c) channel-base current. SL= stepped leader, DL= dart leader, RS = return stroke. From Rakov & Uman (2003).

contact with the ground. These cloud discharges include (1) intracloud discharges, those occuring within the confines of a thundercloud, (2) intercloud discharges, those occuring between thunderclouds and (3) air discharges, those occuring between a thundercloud and clean air. From the observed polarity of the charge effectively lowered to ground and the direction of propagation can CG lightning be further subdivided into (i) downward negative lightning, (ii) upward negative lightning, (iii) downward positive lightning and (iv) upward positive lightning. In fact, there is an additional fifth CG lightning type being the bipolar CG lightning. Observations have shown that the majority of lightning discharges are of type CC, however the magnitude of the involved current is much less than what is observed in CG lightning. In Fig. 6 the typical emitted radiation at low and high frequencies is plotted in case of a CG and CC stroke. It is seen that the emitted radiation in the low frequencies (around 10 kHz) characterizes the return-stroke of a CG lightning discharge, as a result of the large amount of charge carried by the return stroke. On the other hand, radiation associated with CC flashes is made out of hundreds of very fast transient pulses radiating mainly in the VHF (see Fig. 14).

Lets focus for this moment on the downward negative lightning discharge to the Earth's surface, as this type accounts for about 90 percent of all the CG discharges. In a later paragraph, we will briefly discuss other different lightning discharges observed in the Earth's atmosphere. Lets first start with some terminology. A lightning discharge occuring within a cloud or between different clouds is usually termed a lightning *cloud flash*. A *cloud-to-ground flash* is the type of lightning flash occuring between the cloud and the ground, and is simply referred to as a *flash*. A lightning discharge that hits an object on Earth or in the atmosphere, e.g., an airplane, is called a lightning *strike*. A *stroke* is attributed only to CG discharges, where each stroke consists out of a downward leader (stepped leader or dart leader), a return stroke, some continuing current, and various J- and K-components, which are explained in more detail further below. A flash typically contains three to five strokes, with the observed multiplicity being one to 26. When the electric field in a thunderstorm is greater or equal than the breakeven field, as described in Section 2.1, an ensemble of free electrons move as one to create a *leader* which develops into a conducting path between the cloud charge source and the ground. Thus, the latter is a negatively charged plasma channel which serves to transport the charge from within the cloud to the ground. Because the leader develops in virgin air it follows the way of least resistance. As a result, it is an optically intermittent process. Therefore, the first-stroke leader is
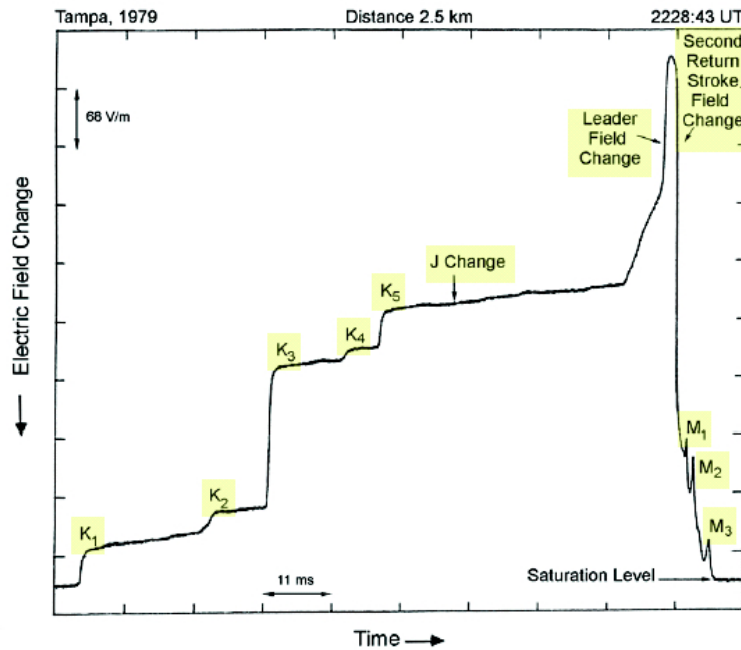
11

Figure 8: A portion of the electric field record for a flash that occurred in Florida in 1979 at 2228:43 UT at a distance of 2.5 km. Labeled are five K-changes (K_1 through K_5), a J-change, leader and return-stroke field changes, as well as three field changes due to M-component (M_1 through M_3). Adapted from Thottappillil et al. (1990).

also termed the *stepped leader* (SL). The stepped leader bridges the distance between cloud and ground with an average speed of $2 \times 10^5 \, \text{ms}^{-1}$ in a series of discrete steps. Each of these steps has a duration of $1 \, \mu s$, resulting in a length of some tens of meters. Note that the peak current attributed to each step is on the order of 1 kA or larger. Subsequently, the stepped leader distributes several Coulombs of negative charge along its path, with a median value of 4.5 C. From this it follows that for a channel length of 6 km, the average charge per unit length is $7 \times 10^{-4} \, \text{Cm}^{-1}$.

Once the stepped leader approaches ground, the electric field at ground is locally enhanced. In particular, this is the case for high buildings and topographic features such as hills and mountains protruding above the surrounding terrain. Once the enhanced electric field exceeds the critical value for initiation, one or more positive upwarded leaders shoot from ground towards the stepped negative leader. An upward leader that makes contact with a branch of a downward leader is called an *upward connecting* leader. The attachment process starts some tens of meters above ground when contact is made between the downward and upward moving leader(s), after which the first *return stroke* (RS) begins. This contact is called the *break-through* phase or *final jump*. At this moment, negative charges at the bottom of the channel move with great speed towards the ground, causing large currents to flow. This, in its turn, causes the luminosity of the channel near ground to increase dramatically. Since the electrons have limited speed the channel luminosity propagates up the channel towards the cloud base, resulting in an optically upward-moving stroke. The return stroke serves to neutralize all the leader charge albeit may not deposit all the leader charge. The speed of the return stroke varies between one-third and one-half the speed of light. The first return-stroke current peaks around 30 kA in some microseconds and decays to half-peak value in some tens of microseconds while exhibiting a number of additional smaller peaks, probably associated with the branches. One side effect of the high-current return-stroke wave is the heating of the channel to temperatures on the order of 30 000 K. This creates a channel pressure of 10 atm or more, resulting in channel expansion and an outward moving shock wave, known as the thunder. Note that the return-stroke is the optically brightest process visible, and produces the most readily identifiable electromagnetic signature.

In a few cases, the lightning discharge stops after the first return-stroke and associated in

-cloud discharges. In this case, the lightning is called a single-stroke flash. The majority of the lightning discharges, however, exhibit further activity. In this case, a subsequent leader follows the first-stroke channel. As a result, this leader moves continuously along the preconditioned path, hence the name downward-moving *dart* leader. Similarly to the development of events leading to the first RS, once the dart leader approaches ground a subsequent return stroke is launched. The speed at which the dart leader progresses towards the ground is on the order of $10^7 \, \text{ms}^{-1}$, and deposits a total charge of around 1 C along the channel, with a dart leader current peak of typically 1 kA. Just as in the case of the first-stroke leader, an attachment process takes place as the dart leader approaches ground. However, now, this occurs over a shorter distance, with the upward

Figure 9: Cumulative statistical distributions of return-stroke peak currents from measurements at a tower top (solid curves) and their log-normal approximations (dashed lines) for (1) negative first strokes, (2) negative subsequent strokes, and (3) positive first (and only) strokes, as reported by Berger et al. (1975).

connecting leader on the order of some meters. Once the connection between the dart leader with the ground is made, another return-stroke wave is launched upward and serves to neutralize the dart leader charge. This gives rise to typical currents on the order of 10 to 15 kA in less than a microsecond and decays to half-peak value in a few tens of microseconds. The processes described above are plotted in Fig. 7. The impulsive component of current of the return stroke may be followed by a continuing current of some 100 A to a few kA lasting for milliseconds. The source for the continuing current differs from that of the return stroke. Now the cloud's charge, as opposed to the charge distributed along the channel in case of the return stroke, is the source and results into a steady charge flow towards the ground. The time interval between successive return strokes in a flash is usually several tens of milliseconds, and can be extended to hundreds of milliseconds depending on the length of the continuing current. Hence, the total duration of a flash varies between a few milliseconds to even a few seconds, lowering a total charge to ground between 1 and 200 C, with a typical value of some tens of Coulombs (Ogawa 1995). Owing to their relatively large charge transfer, continuing currents are responsible for most of the serious lightning damage, such as burned holes or forest fires. Additionally, during the end of the first (or subsequent) return strokes and the initiation of a dart leader, J- and K-processes take place in the cloud. J-processes can be viewed as a relatively slow positive leader extending from the origin of flash initiation[8] into the negative charge region, whereas the K-process begins at the tip of the positive leader and propagates towards the flash origin. K-processes may be viewed as attempted dart leaders, as it serves to transport additional negative charge into and along the existing channel, although not all the way to the ground. An example of an electric field record for a flash exhibiting J- and K-processes is plotted in Fig. 8.

The lightning peak current distributions for negative first and subsequent strokes are shown in Fig. 9. The ordinate gives the percentage of peak currents exceeding the corresponding value on the horizontal axis. One can see from this figure that the median return-stroke current peak for first strokes is two to three times higher than that for subsequent strokes. Only a few percent of negative first strokes are expected to exceed 100 kA, while about 20 percent of positive
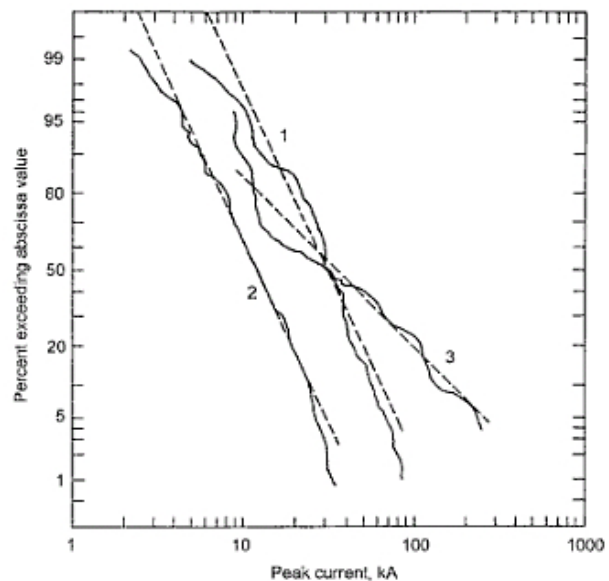
---

[8]Systems for mapping lightning in three dimensions have been used to determine the origin of lightning. In their analysis of mapped lightning from four small, severe thunderstorms in Oklahoma, Rust et al. (1985) used the first mapped point from each flash as the point of origin. They reported that the origins of CG lightning averages just below 7 km, whereas intracloud flashes originated at about 10 km.

Table 1: Some parameters of downward negative lightning derived from channel-base current measurements. Adapted from Berger et al. (1975)

Parameters	Units	Sample size	Percentage exceeding tabulated value		
			95%	50%	5%
Peak current (minimum 2 kA)	kA				
First strokes		101	14	30	80
Subsequent strokes		135	4.6	12	30
Charge (total charge)	C				
First strokes		93	1.1	5.2	24
Subsequent strokes		122	0.2	1.4	11
Complete Flash		94	1.3	7.5	40
Maximum dI/dt	$kA\,\mu s^{-1}$				
First strokes		92	5.5	12	32
Subsequent strokes		122	12	40	120
Stroke duration	μs				
First strokes		90	30	75	200
Subsequent strokes		115	6.5	32	140
Time interval between strokes	ms	133	7	33	150

strokes have been observed to do so. However, the 50 percent (median) values of the current distributions for negative and positive strokes are similar.

Finally, some important lightning parameters are summarized in Table 1. It can be seen that the median return-stroke current peak for first strokes is two to three times higher than for subsequent strokes. Also, negative first strokes transfer about a factor of four larger total charge than do negative subsequent strokes. On the other hand, subsequent return strokes are characterized by three to four times higher current maximum steepness.

2.3   Other types of lightning discharges

In this section, we briefly highlight various other forms of lightning discharges that are observed during thunderstorm activity around the world.

(i) *Positive lightning discharges to ground*: As negative flashes transport negative charge to ground, positive flashes are those who transport positive charge from cloud to the Earth's surface. Positive lightning discharges (PLDs) are thought to account for about 10% or less of the overall global lightning activity, but the highest measured lightning currents (near 300 kA) and the largest charge transfers to ground (>100 Coulombs) are thought to be associated with them, leading to more severe damage to various objects. PLDs can be produced during the dissipating stage of a thunderstorm, after which much of the negative charge has been removed by negative ground flashes. Another mechanism to initiate positive lightning was suggested by Brook et al. (1982) in which PLDs originate from the upper positive charge that can be displaced horizontally by vertical wind shear from the lower negative charge and therefore is exposed to the ground.

It is found that positive flashes can be characterized by the following properties: (a) Positive flashes are usually composed of a single stroke, whereas about 80% of the negative flashes contain two or more strokes. (b) Positive return strokes tend to be followed by continuing currents that typically last tens to hundreds of milliseconds. (c) Often, positive return strokes appear to be preceded by significant in-cloud discharge activity. (d) Positive lightning discharges often involve long horizontal channels, up to tens of kilometers in length. (e) Positive leaders can either be stepped or continuous, in contrast with negative leaders. We refer the interested reader to an in depth review by Rakov (2003) on positive lightning discharges for additional information on this subject.
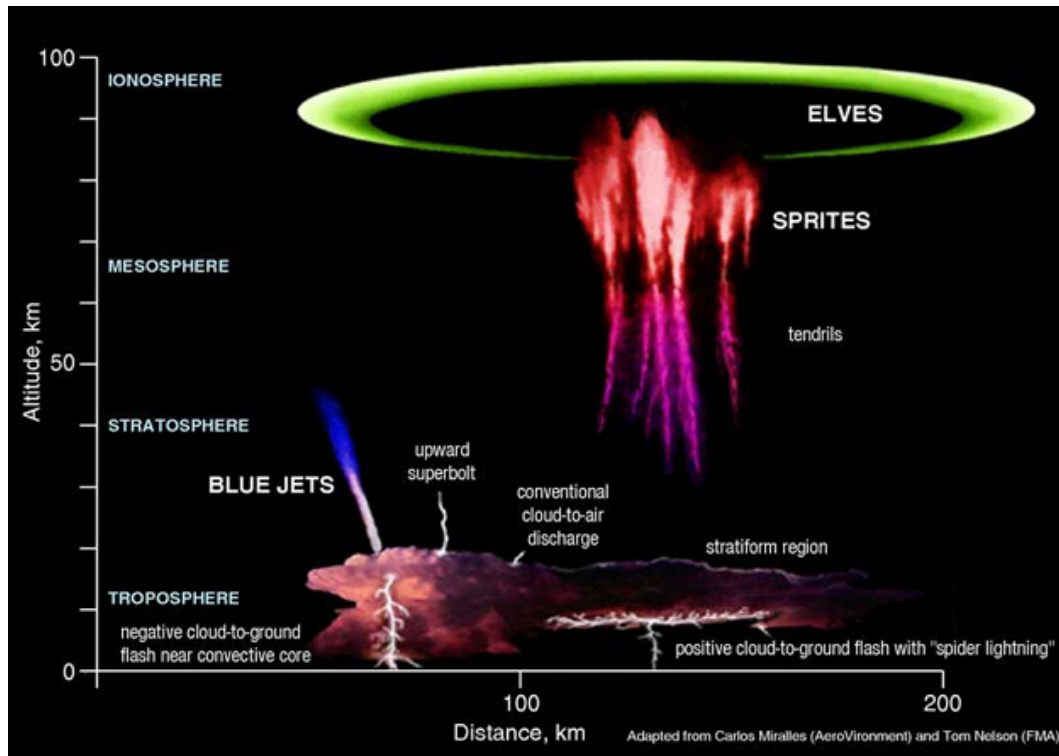
Figure 10: Transient Luminous Events (TLEs) as a function of size and altitude in the atmosphere.

(ii) *Lightning from ground-based objects*: Upward lightning would not occur when a tall object is not present, hence can be considered to be initiated by the object itself. It was first characterized by McEachron (1939), who recorded lightning currents and associated time-resolved photographic images at the Empire State Building in New York. Tall objects with heights from approximately 100 m to 500 m experience both downward and upward flashes, with the ratio decreasing with increasing height of the object. In other words, upward flashes are usually neglected for structures lower than 100 m, and downward flashed are neglected for structures taller than 500 m. Note that if a structure is located on top of a mountain, its effective height is larger than its physical height.

An object-initiated discharge occurs solely when the electric field intensity over a critical distance from the tip of the object exceeds the breakdown value. This critical distance has been found to be around 15 m for objects with a height between 50 to 300 m (Bazelyan et al. 1978). Thus, the existence of an electric field intensity higher than the breakdown value at only the tip of the object or over a shorter distance than 15 m is insufficient for the initiation of a upward lightning discharge.

(iii) *Lightning effects in the middle and upper atmosphere*: Transient Luminous Events (TLEs) is the collective name given to a wide variety of optical emissions which occur in the upper atmosphere above active thunderstoms. They are believed to be the result from a discharge process that develops in the upper atmosphere following a CG lightning discharge in which very large quantities of positive charge (>100 Coulombs) and occasionally negative charge are transferred to ground. They can be understood as a return stroke that does not end in the cloud, but continues to move upward reaching the lower ionosphere. This current causes more exotic forms of lightning to occur, i.e., blue starters/jets, sprites and elves, between the top of the cloud and the lower ionosphere. The relevant scale lengths range from tens of meters to tens and hundreds of kilometers, while the temporal scales range from hundreds of μs to hundreds of ms. The overall understanding of these recently observed phenomena is still in progress, and many details concerning their chemical effects in the atmosphere are not understood to date (e.g., Enell et al. 2008; Sentman et al. 2008).

Blue jets (BJs) are slow moving fountains of blue light from the top of the cloud of active thunderclouds up to altitudes of ∼50 km, whereas *blue starters* (BSs), are brief upward jets which propagate only a few km and terminate below 26 km (Wescott et al. 1996). These luminous flashes were first observed in the 1990s (Franz et al. 1990; Lyons 1994; Sentman & Wescott 1993; Vaughan et al. 1992).

Sprites appear as a cluster of short lived (∼50 ms) red luminous columns, stretching from 30 to 90 km altitude (Sentman et al. 1995). Boccippio et al. (1995) showed that around 80% of sprites are associated with extremely-low-frequency (ELF) events and positive CG lightning return strokes having large peak currents.

Elves are lightning induced flashes that occur higher up, around 90–95 km above ground. They can spread over 300 km laterally in the lower ionosphere. They are the result of the interaction between the propagating Electromagnetic Pulse (EMP) from the lightning and the ionosphere (Inan et al. 1997), and have not been found to correlate with the polarity of the parent lightning.

In Fig. 10 the above described TLEs are plotted as a function of size and altitude in the atmosphere.

3 Locating the source

From a meteorological point of view, the use of atmospherics[9] to track regions of thundery activity provides valuable information on the instability of air masses and the location and movement of fronts. It is clear that this information is of great importance for instance to aviation, since thunderstorms can cause unstable air motions, such as downbursts and microbursts, leading to major difficulties in the take-off and landing of the airplane. Additionally, it is very dangerous to fuel the aircraft while lightning activity is approaching the airport, with the possibility of lightning striking the aircraft. Other sectors also profit from accurate lightning information, such as power plants and public transport services (in particular the train network), whom are vulnerable to direct hits. Evenmore, nowcasting the motion and severity of a storm (linked to the storms electric activity) may lead to the broadcast of a general warning to the public to caution for the approaching hazard. For these reasons it is important to be able to locate the lightning activity in great detail.

All lightning processes are associated with the motion of charge and, therefore, can be studied via measurements of the electric and magnetic fields associated with that motion. As discussed in Sect. 2.1 and 2.2, various physical processes take place in CG and CC flashes, each having an associated radiating electric and magnetic field. These processes, that compose together the lightning stroke/flash, emit electromagnetic pulses with a frequency range that spans from below 1 Hz to near 300 MHz, with a peak in the frequency spectrum around 5–10 kHz. Obviously, electromagnetic radiation from lightning is detectable at even higher frequencies than the ones just mentioned, as in the optical (from 10^{14} to 10^{15} Hz) the lightning appears at the sky as the brightest feature to the human eye. The type of information that can be retrieved from observations depends on the frequency f, and thus wavelength λ, of the detected radiation. For a signal with f = 30 to 300 MHz (λ = 10 to 1 m), that is the very-high-frequency (VHF) range, the wavelength is very short compared to the length of the lightning channel. Hence, the entire lightning channel can in principle be mapped with VHF signals. On the other hand, signals coming from the very-low-frequency (VLF) range (f = 3 to 30 kHz, λ = 10 to 1 km) and low-frequency (LF) range (f = 30 to 300 kHz, λ = 1 km to 100 m) are not suitable to map the lightning channel, but can be used to determine the location of the lightning strike.

Current techniques offer the opportunity to determine various characteristics of the thunderstorm activity, e.g., polarity, multiplicity, strength, and location of the lightning discharge. In the following, we give an overview of the different lightning location system (LLS) techniques to observe lightning discharges.

3.1 Magnetic field direction finding

This technique makes use of Lenz's law[10] of electromagnetic induction to obtain the direction of the source. For this, two vertical magnetic loops are used, positioned orthogonal to each other, oriented along the NS and EW direction. In order to understand how the magnetic field direction finding (MDF) operates, lets first recall the basic idea behind Lenz's law. It tells us that a coil experiences an induced current when the magnetic field passing through it changes. Thus, if the magnetic flux through a loop of wire changes for any reason, either by changing the area A of the loop or by modifying the magnetic field B, than an electromagnetic force (EMF) ϵ is induced in the wire if the loop is closed, which causes a current to flow. It was shown by Lenz that the magnitude of the induced voltage can be written as

$$
\epsilon = -N\frac{\mathrm{d}\Phi}{\mathrm{d}t} = -N\frac{\mathrm{d}(BA cos\eta)}{\mathrm{d}t}
$$
$$
= -N\left[A\,cos\eta\frac{\mathrm{d}B}{\mathrm{d}t} + B\,cos\eta\frac{\mathrm{d}A}{\mathrm{d}t} + BA\frac{\mathrm{d}cos\eta}{\mathrm{d}t}\right],
$$

(2)

---

[9]Atmospherics are electromagnetic waves resulting from lightning discharges in the atmosphere.

[10]The law provides a physical interpretation of the choice of sign in Faraday's law of induction, indicating that the induced electromagnetic force and the change in flux have opposite signs.
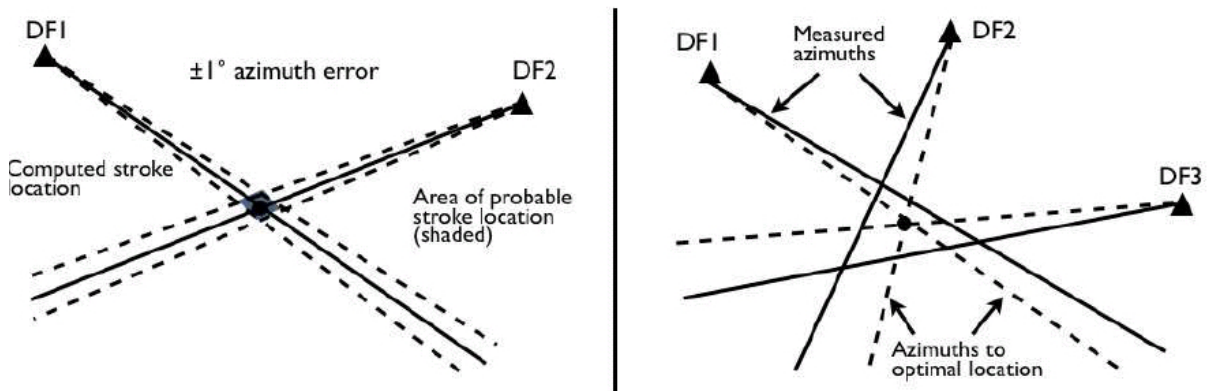
Figure 11: Determination of the lightning stroke location when two (*left*) and three (*right*) direction finders (DFs) detect the stroke. The solid lines represent the measured azimuths to the stroke; the broken line represents the $\pm 1°$ angular random error in the azimuth. The solid circle indicates the computed stroke location. The optimal stroke location is determined by minimizing a χ^2 function. Adapted from Holle & Lopez (1993).

with Φ the magnetic flux through a *single* loop, N the number of turns of wire (each with the same Φ), η the angle between the normal of the magnetic loop and the magnetic field B direction. The first term on the right hand side represents the change in the magnetic field, the second term the change of the loop area. The last term represents the change in orientation of the loop with respect to the magnetic field B. The last two terms are zero, since A and η are constants. Hence, a loop whose plane is oriented NS receives a maximum signal of the source if the source is north or south of the antenna, i.e., $\cos(\eta=0°) = 1$, while the orthogonal loop in EW direction receives no signal, i.e., $\cos(\eta=90°) = 0$. Thus, the signal in the NS loop varies as the cosine of the angle between the north and the source as viewed from the antenna, while the signal in the EW loop varies as the sine of the same angle. Hence, the ratio of the signal of the two loops is proportional to the tangent of the angle between north and the source as viewed from the antenna, i.e., the azimuth angle to the source. A set of MDF sensors are able to locate the position of the lightning discharge. A schematic representation of this (or any other direction finding) method to pinpoint the lightning location is plotted in Fig. 11.

3.2   Time-of-Arrival lightning location retrieval

The name of this technique, Time-of-Arrival (TOA), gives a hint to what method it depends on. It relies on measuring the arrival times of the impulsive emission at a number of antennas in different locations. In Chapter 2 we have seen that a lightning discharge exhibits many different processes, each of which having their own signals. The TOA uses solely the impulsive component of the lightning discharge, i.e., the return stroke peak current, for which a precise time-of-arrival measurement is most easily made at the different antennas. The difference in time-of-arrival between pairs of antennas is used to produce an ensemble of possible locations a stroke hits the ground, which together forms a hyperboloid. The intersection of two hyperboloids gives the direction of the source, whereas three or more time differences are needed to pinpoint the 'exact' location of the source. Fig. 12 plots two different situations wherein the intersection of the hyperboloids, as derived by three different antennas, produce respectively an ambiguous and an exact location. In principle, four stations who detect a signal from the same source are needed to produce a unique location on the Earth's surface. Errors in locations are caused by (i) the identification of different parts of the received waveform at different stations, (ii) path elongation due to mountains, and (iii) inadequate time synchronization between the stations.

It is worth mentioning that this technique can also be used to find the location of the source producing signals in the VHF region of the spectrum. The major difficulty here is the identification and correlation of the numerous impulsive events of a single lightning discharge between the
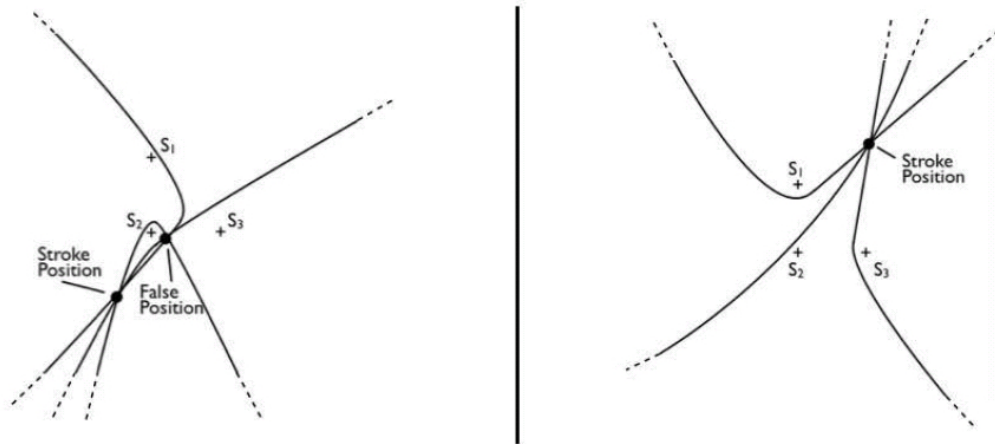
Figure 12: Time-of-arrival (TOA) location technique. The difference of time of arrival for each pair of sensors is confined on a hyperbola. The intersection of the hyperbolas gives the source location. *Left*: example of an ambiguous location for a three-sensor hyperbolic intersection. A fourth sensor is needed to pinpoint the exact location. *Right*: unambiguous location using the hyperbolic intersection method for lightning using three sensors.

various sensors of the system. A prerequisite to succesfully apply the TOA method to VHF signals is that the receivers are spaced in such a way that the time difference between the arrival of an individual VHF pulse from lightning at those receivers is short compared with the time between pulses, which is some microseconds to hundreds of microseconds. Hence, ideally the receivers are separated by tens of kilometers. If the emissions are separated by a period shorter than the baseline between the sensors, the sequence of impulses may not arrive at each sensor in the same order depending on the location of the lightning discharge w.r.t. the sensor location, making the identification process a daunting task. However, Oetzel & Pierce (1969) were the first to successfully use the TOA technique to apply it to VHF sources, and was followed by many others, e.g., Cianos et al. 1972, MacClement & Murty (1978), Taylor (1978) & Maier et al. (1995). Note that in this way it is possible to retrieve a three-dimensional location of the lightning channel.

3.3 Interferometric lightning location retrieval

In addition to the LF impulsive component of the lightning discharge, for which the TOA method makes predominantly use, lightning also produces noise-like bursts of electromagnetic radiation in the VHF region of the spectrum. The data coming from these bursts are hard to reduce using the TOA technique described in previous section, owing to the difficulty in identifying individual pulses. When using interferometric techniques to retrieve a direction of the source, the identification of the individual pulses is not needed, since only the phase difference between signals corresponding to these bursts received by two or more closely spaced sensors is required, typically integrated over 10s of μs.

Lets recall that the phase of a pulse is the fraction of a complete cycle corresponding to an offset in the displacement from a specified reference point at time $t = 0$. On the other hand, a pulse is a harmonic motion that varies cyclically in time and is described by

$$x(t) = A\sin(2\pi f t + \phi), \tag{3}$$

with A the amplitude, f the frequency, t the time and ϕ the phase; with one wavelength corresponding to 360° or 2π radians.

In Fig. 13, the simplest configuration consisting out of two receivers using interferometry is plotted. Using the coordinate system of Fig. 13, the phase difference between a signal whose
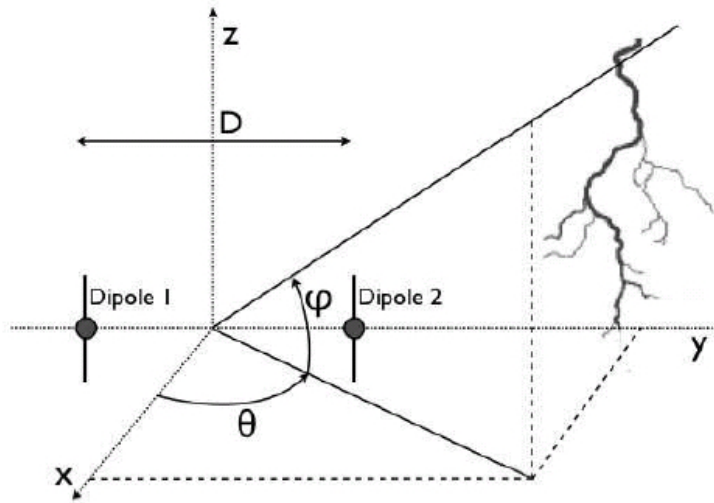
Figure 13: Illustration of the coordinate system for a spaced interferometric pair of dipoles, illuminated by a monochromatic wave. The azimuth of the source θ and elevation angle φ are depicted.

wavelength λ is caught by two dipoles situated at the same altitude and separated by a distance D will be equal to:

$$\delta\phi = 2\pi \frac{D}{\lambda}\sin\theta\cos\varphi. \tag{4}$$

The placement of a second interferometric pair orthogonal to the first, such that the azimuth θ will be rotated by 90°, results in a transformation of the sine to the cosine. We therefore find that:

$$\begin{cases} \delta\phi_1 = 2\pi\frac{D}{\lambda}\sin\theta\cos\varphi \\ \delta\phi_2 = 2\pi\frac{D}{\lambda}\cos\theta\cos\varphi \end{cases} \tag{5}$$

The unknown azimuth θ follows out of the ratio of the two phase differences. Note that the angular accuracy of such a network is related to the accuracy of the phase measurement. The data set of these interferometric sensors are transported to a central processor which locates each individual event by triangulation[11]. The use of VHF radiation is limited to local lightning activity in thunderstorms due to the significant attenuation of the signal with distance. Despite networks based on VHF signals cannot provide information over large regional areas, these systems can provide information on the storm development, intensity and possibility of severe weather and are therefore invaluable for early warning systems.

3.4   Ground-based optical direction finding

The use of optical signals to determine the direction of the lighting discharge is not without its complications. The lightning channel for instance can be (totally or partially) obscured by topography, precipitation, clouds, trees, and buildings. Nevertheless, this method, making use of state-of-the-art optical sensors (photographic and/or video), has been successfully applied by, e.g., Kidder (1973), Winn et al. (1973), Rakov et al. (1994), and Idone et al. (1998a, b), to determine the lightning location by triangulation, as well as lightning properties such as the number of strokes per flash, the number of separate channels to ground per flash, and the flash duration. These observations are further hampered by the shutter action and time resolution of the optical sensor.

---

[11]Triangulation is the process of determining the location of a point by measuring angles to it from known points at either end of a fixed baseline. The location of the lightning discharge can then be fixed as the third point of a triangle with one known side and two known angles.

3.5   Satellite observations

Satellites orbiting the Earth have the possibility to detect worldwide lightning activity within thunderstorms by detecting the light emitted in the upward direction. Satellite sensors eliminate the potential problem of predominantly land-based sensors biasing the measured oceanic and continental fractions. Lightning observations from satellites have been already possible from the 1980s, with the launch of two satellites with photographic detectors as part of the Defense Meteorological Satellite Program (DMSP) (Orville & Spencer 1979; Orville 1981). These satellites were not able to detect large fractions of the lightning activity in a thunderstorm due to their low orbit and hence short time over any given thunderstorm. Nevertheless, it was possible to determine ratios of activity in different geographical regions and seasons. For instance, Turman & Edgar (1982) estimated that at dusk 15% of flashes were from oceanic storms and 85% from continental storms, while at dawn 37% (63%) were from oceanic (continental) thunderstorms. This can be explained by the fact that at dusk the highest convective activity is situated over land. On the other hand, the activity of thunderstorms over land decreases during the night and reaches its minimum at the end of the night and at dawn, while thunderstorms over sea do not experience such a decrease of activity as the sea surface temperature stays roughly constant. It was followed up in the 90s by a lightning mapper, developed by NASA researchers, designed for geostationary orbit (Davis et al. 1983; Christian et al. 1989). The system is able to both map ground and cloud lightning continuously. At around the same time, Meteosat First Generation satellites were launched (1977–1997, Meteosat-1 to 7) to play a key role in the continuous atmospheric observations. The second generation of Meteosat satellites is expected to be operational until 2015, and plans are already made for the third generation of satellites. The latter will have a *Lightning Imagery* (LI) mission, designed to map continuously lightning discharges into geostationary orbit with a spatial resolution of 10 km. The technique for doing so is based on the detection of the strongest lightning emission feature within the cloud-top optical spectra produced by the neutral oxygen line at 777.4 nm. In addition, the Tropical Rainfall Measuring Mission (TRMM) launched in 1997 with on board the Lightning Imaging Sensor (LIS) is worth mentioning. The LIS is a compact combination of optical and electronic elements which allows to observe a point on the Earth or a cloud for 80 seconds, a sufficient time to estimate the flashing rate, which tells researchers whether a storm is growing or decaying. As such, it is clear that satellite data can help weather forecasters in detecting severe storms in time.

3.6   Radar observations

We have seen in Sect. 2.1 and others that lightning emits in a very wide range of frequency space. Lightning discharges can be detected also via radio-observations, since lightning channels are highly reflective at radio frequencies. Therefore, radar can be used to detect electromagnetic radiation from the lightning flash. The observation of lightning with weather radars was first conducted in the 1950s, e.g., Ligda (1950, 1956), Browne (1951), and only recently have radars been used specifically to locate lightning, determine physical characteristics of channels, and relate lightning to storm evolution (Cerni 1976; Holmes et al. 1980; Mazur 1986). For a thorough review on radar studies of lightning, we refer the interested reader to Williams et al. (1990).

The longer the wavelength of the radar, the less reflective the precipitation and the easier it becomes to detect lightning in precipitation. In practice, the wavelength needs to be at least 10 cm to avoid excessive precipitation masking of the echoes from lightning. Longer wavelengths of up to a meter or two reduce the precipitation return even more. One way to observe lightning is to aim a stationary (non-scanning) radar antenna at an active region of a storm. Radar location of lightning can then be conducted using simultaneous observations of a set of radars. On the other hand, the use of a single radar can provide information on the channel characteristics.

It is worth mentioning that the use of radar could be even superior, with respect to the TOA and interferometric techniques, because it can still detect low-level radiation from the current-carrying channel, that would fall otherwise under the threshold levels of aforementioned methods. This was noted by Williams et al. (1990). However, to map the lightning channel in

three dimensions, a radar with high spatial and short-time resolution is required. Such a radar is currently not in operation, even being technically feasible at the moment. Nevertheless, a less than optimal radar system can provide useful lightning information, especially when coupled to other locators.

3.7   Global lightning information from Schumann resonances

In the extremely-low-frequency (ELF) range (3–300 Hz), radio waves from lightning undergo little attenuation and hence manage to propagate around the globe a number of times before decaying into the background noise. As a result, an interference[12] between the *direct* and the *around-the-globe* wave occurs, in a phenomenon called the Schumann[13] resonances[14] (SRs). The reason for this is that the surface and conductive ionosphere of the Earth form a cavity that, when excited with a broadband electromagnetic spectrum, can develop resonant states if the equatorial circumference is approximately equal to an integral number of wavelengths of the propagating electromagnetic wave. The source of the electromagnetic spectrum can be provided by lightning activity. As a result, the weak lightning signals below $\sim$100 Hz are amplified at the resonance frequencies. A simple approximation to estimate the Schumann frequencies is to consider this cavity. It can be shown that if the terrestrial waveguide was an ideal one, the Earth-ionosphere cavity eigenfrequencies ω_n are given by

$$\omega_n = \sqrt{n(n+1)}\frac{c}{2\pi R},$$

(6)

where c is the speed of light in the cavity, R the cavity radius, and n an integer (Schumann 1954, 1957). However, the Earth-ionosphere waveguide is not a perfect electromagnetic cavity. Losses due to finite ionosphere conductivity make the system resonate at lower frequencies than would be expected in an ideal case. These frequencies correspond to the resonant modes of the cavity (Schumann resonances) and fall within the ELF range for the Earth. Schumann resonances are the principal background in the electromagnetic spectrum between 3–69 Hz, and appear as distinct peaks at ELF around 7.83, 14.3, 20.8, 27.3 and 33.8 Hz. Note that the excitation of the cavity by lightning can occur as a single energetic flash (Q-burst), or as an integration of a large number of less energetic flashes (background resonances). It is out of the scope of this manuscript to go into the many details of how to extract lightning information from Schumann resonance observations. However, it is important to know that in principle the continuous observation of SR parameters (amplitudes, frequencies, ...) provides invaluable information for monitoring worldwide lightning activity, as Schumann resonances exhibit amplitude and frequency variability related to the location of lightning (e.g., Nickolaenko & Hayakawa 2002).

3.8   Discrimination between cloud-to-ground versus intracloud lightning

A lightning flash is a broadband electromagnetic radiator. Ground flashes have a strong, low-frequency component associated with the initiation of the return stroke, with the peak in frequency around 10 kHz. This is one reason why a broadcast band AM radio tuned to its lower end works as a rudimentary lightning detector. The amplitude of the different frequencies varies during a flash and is dependent upon the process(es) under way at any instant.

The electric field change for a lightning flash is a fundamental measurement made in many lightning and thunderstorm studies because the field change for the whole event can often reveal important physical parameters as well as distinguish between a cloud or ground flash.

---

[12]Interference is the superposition of two or more waves that results in a new wave pattern.

[13]After the German scientist Schumann who predicted them theoretically in 1952.

[14]Resonance is the tendency of a system (usually a linear system) to oscillate at larger amplitude at some frequencies than at others.
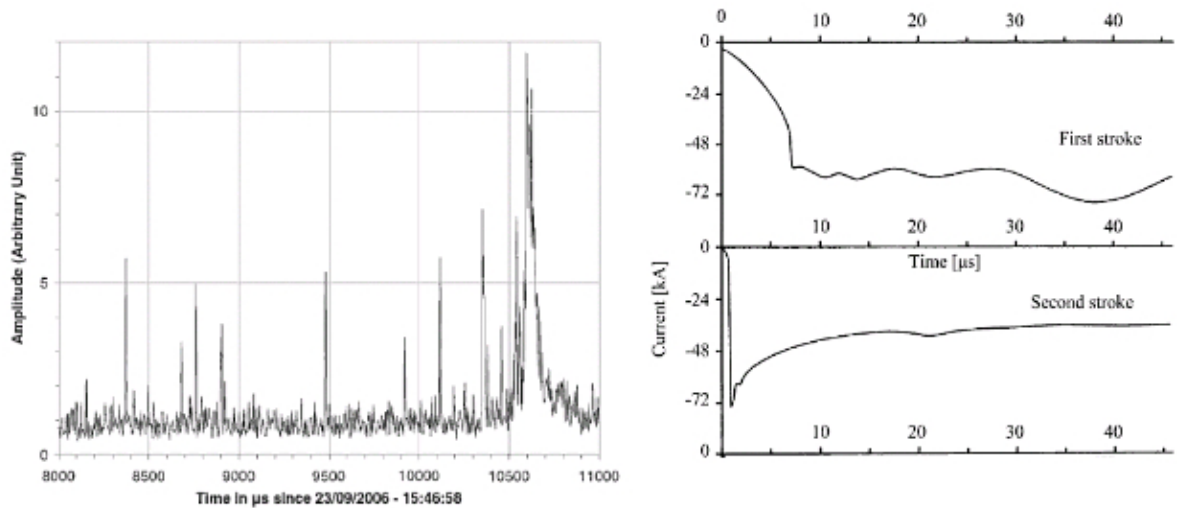
Figure 14: *Left*: Typical VHF waveform showing impulsive radiation events and one continuous burst of radiation lasting for about $300\,\mu s$. Adapted from Lojou et al. (2008). *Right*: Return stroke current observed at ground for a first and subsequent stroke lowering negative charge to a 60 m tower standing on flat ground in South Africa. Adapted from Eriksson (1978).

The discrimination between CC and CG is based on the shape and amplitude of the waveform, i.e., the rise and decline times, measured by the sensor through the change in electric field strength. These changes are strongest for CG discharges, where the decline time is the most important parameter. When the electric field strength reaches a certain threshold value, and rises further to a previously determined validation threshold, one can assume the electric field is due to a CG discharge. This is because, CC discharges produce, as a result of the moderate current flow, weaker LF radiation signals compared to CG discharges. From this, one is able to determine the current. According to Uman et al. (1975) the peak current of the return stroke I_p is related to the measured electric strength peak E_p by the sensor and to the return stroke speed v through the following expression:

$$I_p = \frac{2\pi\epsilon_0 c^2 D}{v} E_p, \tag{7}$$

with D the distance between the sensor and the ground contact point of the lightning stroke, c the speed of light and ϵ_0 the electric constant.

Some lightning location systems are designed to detect and differentiate between CC and CG stroke lightning events, and are based on the fact that CC lightning generates much higher short-term energy at higher frequencies than CG strokes. This information is beneficial in identifying and displaying storm cells that contain cloud-to-cloud lightning. Detecting both types of events provides a better overall picture of the storm activity and allows improved analysis of storm development and decay. Fig. 14 plots a typical VHF waveform, in addition to a typical current waveform for negative downward lightning. The VHF waveform clearly exhibits several narrow pulses occuring together with a more continuous process whose duration is about $300\,\mu s$, whereas the waveform for downward negative lightning displays a more smooth behavior.

3.9   Detection efficiency, location accuracy, & false alarm rate

The important performance characteristics of any lightning detection system can be classified into three categories: (i) detection efficiency (DE), (ii) location accuracy (LA), and (iii) false alarm rate (FAR). In the following, we briefly explain the different classifications.

Table 2: Lightning Location System characteristics

Sensors	Frequency [Hz]	Location Techniques	Spatial Coverage	Location Accuracy	Type of Lightning Detected	Detection Efficiency [% of total]
VHF	$\sim 10^8$	TOA, IF	Local	meters	Total: CC, CG	$>90\%$
VLF	$\sim 10^4$	TOA, MDF	Regional	kilometers	mainly CG	$<25\%$
ELF	~ 10	MDF, Schumann resonance	Global	Megameters	CG	$<5\%$

(i) *Detection Efficiency (DE)*: the DE of a network is the ratio of the number of detected events divided by the real number of events that have actually occurred. It is not surprising that a DE of 100% for any operating network is nearly impossible to achieve, due to sensor faults, communication problems and/or an unfavorable network geometry (Naccarato 2005). This may lead to misinterpreting the data over long periods in time. As such, the DE of a network can be a major limitation of the system; a high DE is highly recommended.

The first step in determining the DE of a network is to compute the relative detection efficiency (RDE) probability distribution for each sensor. The sensor RDE distribution corresponds to the ratio between the number of CG flashes reported by the particular sensor and the total number of CG flashes detected by the network. The RDE is a function of peak current, e.g., 5 kA, 10 kA, etc., and of the distance to the event. Using the calculated RDE for each sensor, a network DE can be computed based on the combined probability of each sensor to detect an event or not, considering its distance from each sensor. If for instance a relative modest peak current of 10 kA is attributed to a specific lightning strike, it is possible that, at a certain distance from the event, the sensor does not recognise it as a lightning event. As a result, information can be lost when the minimum number of sensors required to produce a solution is not reached, e.g., four stations who detect a signal from the same source are required to produce a unique location based on TOA. However, an event striking at the same position with a peak current of 40 kA can be strong enough to trigger the sensor. The detection efficiency of the network will be reduced when the lightning stroke occurs outside of the network or when not all of the stations are operative. An increase in DE is readily achieved by increasing the number of active stations.

Note that for a network using both LF and VHF observations, an *effective* DE for the VHF system can be determined when considering CG strokes reported by the LF network as ground truth. The VHF system does not directly measure return strokes of CG strokes, but they do detect other associated discharges which occur as part of a CG stroke. Hence, a VHF network is said to have detected a CG stroke reported by the LF network if it locates at least one source within a certain time and spatial interval. A simple count of such events divided by the actual number of CG strokes observed by the LF network provides an estimation of the effective CG stroke detection efficiency of the VHF system.

(ii) *Location Accuracy (LA)*: this is somewhat more difficult to determine, as the location of a lightning event corresponds to the time when the current reaches its peak value. At that moment, a return stroke is initiated. We have seen in Sect. 2.2 that the attachment point of the downward negative leader with the upward positive leader, activating a return stroke, lies a few tens to even hundreds of meters above ground. Since the return stroke does not move as a perfect vertical channel towards the Earth, the actual ground stroke position can easily differ by up to of few hundred of meters.

In order to determine the LA of a network, one needs to use lightning data for which the exact location is known. For instance, electrical plants and train networks may provide the necessary location and time information of a hit as part of their damage reports. As for the DE, the LA reduces for an event outside the network or when one of the sensors is no longer operational, and may be increased with increasing number of available sensors. In addition, the LA together with the DE can be examined by contrasting its observations with those from neighbouring lightning detection networks.

(iii) *False Alarm Rate (FAR)*: is the partition of wrongly detected non-lightning events. It depends on the signal-to-noise value and the detection threshold of the system. Observations show that lightning discharges do not occur during clear sky, but are always associated with clouds and/or precipitation activity. As such, a criterion in the processing of the data can be implemented to consider an apparent lightning flash as a non-event. For this, radar images of precipitation can be overlayed on top of the registered lightning locations. In case a lightning event is recorded at a considerable distance from a precipitation region, the event can be excluded from the data. It is necessary to choose a certain reflectivity value for precipitation. It is wisely not to choose this value too high, as lightning events can be excluded that are initiated in low-level precipitation clouds. Note that occasionally *dry* thunderstorms, i.e., non-precipitating thunderstorms, exist. In this case, the use of satellite images with respect to the derived lightning location is favorable to distinguish between a real lightning discharge or a non-event.

All these techniques need a number of sensors within a network to retrieve reliable data on the location of the lightning flash, and focus on a particular wavelength band. The highest frequencies are attenuated first, hence lightning detection systems based on VHF radiation are used to study local discharge events. On the other hand, VLF radiation can travel great distances, i.e., thousands of kilometers, and are used for regional observations. This is because the electromagnetic energy propagates with low attenuation inside the waveguide formed by the conducting Earth and the lower boundary of the ionosphere, termed the Earth-Ionosphere Waveguide (EIWG). Finally, it is possible to detect global lightning activity with sensors sensitive in the extremely-low-frequency band (ELF), as discussed in Sect. 3.7. Some characteristics of sensors based on VHF, VLF and ELF are in Table 2. Note that values for the DE are for illustration purposes only, and should not be applied blindly to a specific system at interest.

4 Ground-based lightning detection networks

Lightning is an electrical discharge either within clouds (CC), or between clouds and the ground (CG). As discussed in Chapter 2, the rapid acceleration of charge during the lightning flash generates electromagnetic radiation in a broad frequency band. This radiation propagates away from the channel, with the highest frequencies being attenuated first, while the lowest frequencies travel great distances; even around the globe via extremely-low-frequency (ELF) radiation. For this reason, networks with very-high-frequency (VHF) sensors only detect lightning activity in the vicinity of the network. On regional scales VHF radiation cannot be detected, and (very-)low-frequency (VLF/LF) sensors are used to detect the radiation that manages to propagate thousands of kilometers before decaying. Networks operating over large regions using VLF sensors supply great regional coverage and reasonable spatial accuracy and detection efficiency (depending on the amount and spacing of the sensors). However, VLF/LF sensors are primarily sensitive to vertically oriented lightning discharges. Hence, much of the CC is not detected by these large scale networks.

The techniques as described in Chapter 3 by which VHF, VLF/LF and ELF sensors detect and locate electrical activity in thunderstorms include direction finding (DF), time-of-arrival (TOA), a combination of these two, and interferometry methods. In this Chapter we try to give a concise overview of the different lightning detection networks operating in Europe (§4.1) and some other large-scale networks in the world (§4.2).

4.1 European networks

Here, we present several lightning detection networks operating in European countries and joint cooperations between different countries. Note that the following is not a definitive inventory of all the operating networks and is based on the available information at this moment.

AEMET: the Agencia Estatal de Meteorología (AEMET) in Spain uses 20 Vaisala sensors of the IMPACT[15] type.

ALDIS: the Austrian Lightning Detection and Information System (ALDIS) is a joint project of the Österreichische Verband für Elektrotechnik (OVE), Siemens and Verbund (Austria's largest electricity producer and transporter). The goal of this project is real-time monitoring of lightning activity in the area of Central Europe and provides this information to meteorological services, insurance companies and power utilities. The network consists of eight IMPACT sensors, with a mean baseline of about 120 km. The sensors measure the polarity of the electric field in order to determine the polarity of the flash. Furthermore, the wave angle of the magnetic field as well as the precise time of the signal arriving by the sensor are recorded. ALDIS detects solely CG strokes. The relatively short baseline allows an accuracy of lightning detection of better than 1 km on average (Diendorfer et al. 1992). The detection efficiency of 90% is relatively high over the main part of Austria and decreases at the edges as the distance to the nearest sensor increases.

ATDNET: the United Kingdom Met Office, UK's national weather service, started in the 1980s with the usage of a VLF arrival time difference (ATD) long range lightning location network. The range of the network included all of Europe, North Africa, North Atlantic and most of South America. The system was originally designed to measure cloud to ground strokes over the UK with a location accuracy of about 2 km. It was constructed as a thunderstorm detection system, providing the location of nearly all the thunderstorms in Europe that gave cloud to ground

---

[15]Improved Performance from Combined Technology (IMPACT) sensors use two orthogonal magnetic antennas to determine the incidence direction of a lightning signal, i.e., magnetic direction finding (MDF), and also determines TOA of the signal. IMPACT sensors were developed by Global Atmospherics Inc. Note: Global Atmospheric Incorporated of Tucson, Arizona, USA, has joined Vaisala and was renamed Vaisala-GAI in 2002. The company is now part of Vaisala's Remote Sensing Division.

strokes. The network operated at frequencies around 9.766 kHz with a measured bandwidth of 3 kHz. At these frequencies the sky waves, reflected off the ionosphere, propagate over very large distances with relatively little attenuation and are preceded by a ground wave at shorter ranges. Hence, it is possible to receive emission from the CG strokes at thousands of kilometers from the stroke location. In 2007, the system has been upgraded and the name changed into the Arrival Time Difference Network (ATDNET). The expansions and improvements to the network resulted in an increase of the detectable range of lightning and now includes all of South America, Africa and central Asia. In addition, monitoring in 2004 showed increasing levels of man-made interference around the original centre frequency of 9.766 kHz, and as a result moved to 13.733 kHz. The improved network currently has 14 NOS detectors (NewOutStation) and it is calculated that ~30 sensors would be enough for a global coverage. As such, ATDNET detects mainly ground flashes. These ground flashes are usually the first return stroke, since the system has a 15 ms 'dead-time'[16], unfavorable for the detection of subsequent return strokes. ATDNET cannot detect cloud flashes due to the general weaker signal. Information of the CG stroke does not incorporate flash polarity and peak current. However, as mentioned above ATDNET provides ground flash information with a relatively small number of sensors from large areas.

Studies have shown that the location accuracy increased from 5 km over the United Kingdom and 20 km over the rest of Europe (Keogh et al. 2006) for ATD, to an average accuracy of 2–3 km over Europe and ~5 km in Africa for ATDNET. The detection efficiency varies according to the region with DE up to 90% over UK and Western Europe, DE of 80% over Northern Africa and drops to a DE of 20% in South America. Note that the aforementioned values show a diurnal variation due to the changes in electron density and ground conductivity.

BLDN: a Benelux Lightning Detection Network (BLDN) is operational since 1999, managed by Siemens. The network consists out of six sensors positioned along Belgium, the Netherlands and one just over the border of Luxembourg in France. There are 4 LPATS[17] and 2 IMPACT ESP[18] sensors.

BLIDS: the lightning detection network BLIDS (BLitz InformationsDienst von Siemens) is operated by Siemens AG since 1992. It currently consists of 14 receiver stations in Germany. In addition, being an integral part of the EUCLID network, it uses supplementary data from all other EUCLID stations. The receiver stations are equipped with a mixture of LPATS III, LPATS IV and IMPACT ESP sensors.

Due to the lower frequency range used, LPATS and IMPACT are predominantly sensitive to CG flashes, i.e., the LF signature of the RS is easily detected, and can distinguish between flash polarity. CC detection efficiency is estimated to be 1% (see Théry 2000). Discrimination between CC and CG flashes is made using the decay time (peak to zero, PTZ) of a signal.

CELDN: the Central European Lightning Detection Network (CELDN) is operated by Siemens AG and Vaisala since 2002. It was created by combining the LF sensors from the German BLIDS and Austrian ALDIS network together with several newly installed sensors in Czech Republic, Poland, Slovakia and Hungary. Together the network provides accurate lightning data over the central part of Europe. CELDNs primary goal is targeted on detection of CG lightning, but CC lightning detection is also possible. A location accuracy of approximately 1 km is reached.

CESI-SIRF: the Italian lightning detection network SIRF (Sistema Italiano Rilevamento Fulmini) was installed by CESI (Centro Elettrotecnico Sperimentale Italiano) in 1994. It consists of 16 IMPACT sensors with a mean baseline of about 200 km throughout Italy. The central processor of all the data is located in Milan at CESI. It covers all the Italian territory and the main islands with an estimated detection efficiency of 90% for currents greater than 2 kA up to 200 km, i.e., the baseline of the sensors, and an estimated location accuracy of 1 km.

---

[16]The 'dead-time' of a sensor is the time a sensor cannot process another lightning signal after receiving a signal. As such, signals arriving the sensor during the dead-time are lost.

[17]Lightning Positioning and Tracking System (LPATS) sensors are LF wideband (1–350 kHz) receivers. LPATS sensors use the time-of-arrival (TOA) method for position retrieval. LPATS sensors were developed by Atmospheric Research Inc.

[18]Improved Performance from Combined Technology - Enhanced Sensitivity and Performance

DHMZ: the Meteorological and Hydrological Service of Croatia (DHMZ) is hosting one ATDnet outstation and five LINET sensors are installed. For more information on the principle of LINET sensors, the interested reader is referred to the LINET paragraph in this section.

DMI: the lightning network of the Danmarks Meteorologiske Institut was established in 2000. The extent of thunderstorms is monitored from six lightning detection stations located throughout the country and the location of lightning strikes is identified. The network detects both CC and CG lightning with an estimated accuracy of $\sim$1 km. The system provides important information not only to DMI's Forecasting Services Department, but also to public and private institutions such as power companies, who use the information for fault location, ensuring the safety of cable workers, etc.

EIMV/SCALAR: the Elektroinstitut Milan Vidmar (EIMV) network in Slovenia for lightning detection became operational in 1997 when EIMV and Elektro Slovenija (ELES) joined forces with the help from the Finnish Meteorological Institute whom provided the software. The network consists of two LPATS III sensors which are linked together with the 8 IMPACT sensors from the ALDIS network. This combined lightning location system is called SCALAR (Slovenian Centre for Automatic Localization of Atmospheric Discharges). Incorporation of the SCALAR system into the EUCLID network has improved the system accuracy to an estimated $\pm$500 m and its efficiency has increased to over 80%.

EUCLID: EUCLID (EUropean Cooperation for LIghtning Detection) is a collaboration among national lightning detecting networks with the aim to identify and detect lightning all over the European area. Most of the operational national networks in Central Europe are integrated in the EUCLID network since 2000. They share data and evaluate the measurements in conjunction with some or all other participants in order to assure a continuous high data quality, even in border regions of national systems. As of August 2009, The EUCLID network consists of 137 sensors, under which 5 LPATS III, 18 LPATS IV, 15 IMPACT, 54 IMPACT ES/ESP, 3 SAFIR and 42 LS7000[19] sensors (oldest to newest), operating in the VHF and LF frequency range. Data from all these sensors are processed in real-time using a single common central processor. In addition, this cooperation serves as a platform for exchange of knowledge related to lightning location technology. This network covers 18 countries in Europe (Austria, Belgium, Czech Republic, Finland, France, Germany, Hungary, Italy, Luxembourg, the Netherlands, Norway, Poland, Portugal, Slovenia, Slovakia, Spain, Sweden and Switzerland) and builds a true interconnected network which covers almost all the European continent on a cooperative basis. Networks included in EUCLID are ALDIS, BLDN, BLIDS, CELDN, CESI-SIRF, EIMV, Météorage and NORDLIS.

As with the (American) National Lightning Detection Network (NLDN), the EUCLID network was designed to primarily locate CG flashes. It is found that the flash detection efficiency is higher than 90% in all the participating countries, with a location accuracy of $\sim$500 m throughout Europe. Stroke detection efficiency DE_s is calculated to be 70% for strokes with peak currents in the range from 5–6 kA, whereas DE_s increases to 99% for all strokes with peak current higher than 10 kA.

FMI: the Finnish Meteorological Institute (FMI) employs a lightning detection network consistig out 5 IMPACT sensors and 3 SAFIR 3000 sensors and is a member of the NORDLIS consortium. The system is capable to detect CG and CC lightning (only the 3 SAFIR 3000 sensors are used for the detection of cloud lightning using VHF measurements), but with a poorer DE and LA for the latter. The estimated LA is 500 m in the center and 2 km at the edges of the network.

HNMS: the Hellenic National Meteorological Service (HNMS) of Greece operates a newly installed system since 2008 consisting out eight sensors, being installed by the American manufacturer 'TOA'. The manufacturer claims a 90% DE for CC and CG.

---

[19]This type of lightning sensor (LS) employs low frequency (LF) combined magnetic direction finding and time-of-arrival (TOA) technology.

KNMI: since 1995 KNMI operates a SAFIR lightning detection system consisting out four stations. In addition, sensor data from three Belgian stations operated at RMI are processed in real time as well. Each station consists out of a VHF antenna array, a LF sensor and a GPS receiver. KNMI have developed a central processing system FLITS, different from the Vaisala provided SAFIR processing system. The system has the capability to detect CG as well as CC flashes. The location accuracy is measured to be about 2 km, with a detection efficiency of ∼60%.

LAMPINET: in 2004 the Italian Air Force Meteorological Service (IAFMS) constructed the lightning network LAMPINET. The network was adopted primarily for nowcast of strong electrical activity connected with atmospheric instability and to prevent risks both in air operation and ground activities, such as refueling and power plant protection. The network consists of 15 IMPACT ESP sensors uniformly distributed over the peninsula and the islands. The manufacturer (Vaisala) of the network claims that performances reach a detection efficiency of 90% for a discharge with a peak current superior to 50 kA and location accuracy of ∼500 m in the central regions of Italy; larger errors are expected in the border areas and beyond the network.

LINET:
the University of Munich developed a VLF/LF lightning detection network (LINET), motivated by the needs for improved early recognition of thunderstorms and severe weather conditions. At present, the network comprises about 90 sensors in 17 countries in Europe, from which 30 are placed in Germany. All the receivers in the network are identical, utilize the VLF/LF frequency range, and detect the magnetic flux of the lightning signal by means of two orthogonal loops and serve to infer both amplitudes and angles by the DF method. In Germany, the distance between neighboring sensors is near 200 km or less. The goal is a total lightning system that discriminates between CG and CC discharges on the basis of their VLF/LF

Figure 15: Principle of time delay associated with CC-discharges as compared to CG strokes from the same 2D location. $dT = T_P - T_H$, S = sensor station, P = center of VLF emission and H = emission source height. Adapted from Betz et al. (2009).

pulses only, in contrary to many other networks, e.g., SAFIR-type networks, which employ VHF as well as VLF/LF sensors. LINET, accepts any wave form no matter how complex it is with all prominent peaks identified and time-tagged, since one observes a very wide variation of signal forms.

LINET performs CC-CG discrimination not by means of waveform criteria but by a specially developed 3D-TOA-algorithm in the central processing unit. In this way, LINET circumvents problems related to the finding that shape differences between CC and CG signals become less pronounced when the amplitude decreases. Note that location and measurement of CC events with VLF/LF techniques require that the used network is capable of detecting small pulses, irrespective of the pulse shape. LINET can detect VLF/LF pulses down to ∼2 kA. The algorithm is based on the well-known fact that CG strokes emit VLF/LF radiation dominantly from channel parts close to ground level, while CC emission originates necessarily from channel segments inside clouds and well above ground level. LINET applies first the usual 2D locating algorithm to determine ground locations. Secondly, for the sensor nearest to the lightning the difference dT between the measured event time T_P and the one expected on the basis of travel time between the 2D located point of lightning and the sensor T_H is determined, see Fig. 15. Whenever the emission center is elevated the signal travel time to the sensor is longer as compared with ground wave propagation. Consequently, the arrival time is delayed and should result in a small inconsistency with respect to the results produced by the locating algo-
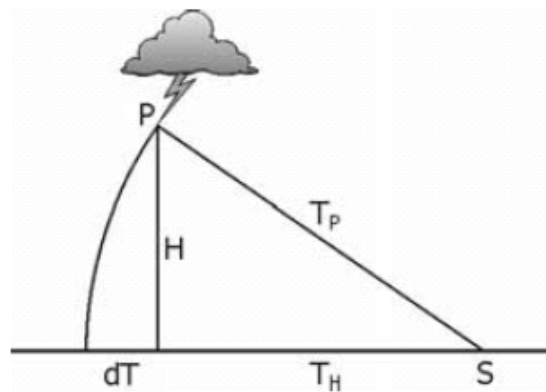
rithm. In other words, the sensor nearest to the lightning does not fit properly into the general picture. Thus, for a CG stroke, this difference is dT=0, however a dT$\neq$0 is characteristic for a CC stroke. For instance, emission from a source height of 10 km produces a TOA-delay of 3.3 μs (1.7 μs) compared with ground level propagation when recorded at a sensor distance of 50 km (100 km). This difference is detectable in modern networks, provided that at least one sensor is not further away from the lightning than $\sim$100 km as GPS based timing networks report event time precision on the order of 1 μs. The discrimination of CC and CG yields thus a characteristic height of CC events. It is verified by means of strikes to towers that the LINET network has a location accuracy of approximately 150 m (Betz et al. 2009).

METEOCAT/SMC: the Catalan Meteorological Service (Meteocat/SMC) operates a lightning detection network (MLDN/XDDE) . The network is composed out of three Vaisala SAFIR sensors, covering the region of Catalonia (NE of Spain), which translates to an area of $\sim$32 000 km^2. The system provides 2D location of VHF (108–116 MHz) sources produced by any lightning flashes (CC and CG), based on interferometry. Studies have shown that the spatial accuracy of the network ranges from 1–2 km at the center of the network, whereas the CG flash detection efficiency of the XDDE was found to be between 86–92% (Montanyà et al. 2006).

METEORAGE: Météorage manages and operates the lightning detection network comprising some 18 Vaisala IMPACT sensors in France since 1996 that work in conjunction with Swiss, Austrian, Italian and Spanish sensors. Location techniques are based on direction finding and time-of-arrival, resulting in an location accuracy to within 1 kilometer everywhere in France and a DE of 90–95%.

NORDLIS: Finland, Norway and Sweden and Estonia joined forces and started the so-called NORDLIS lightning location system, mainly based on Vaisala IMPACT sensors, and is meant for the detection of CG flashes. At present, about 30 sensors are connected to the central unit at the Finnish Meteorological Institute (FMI). In Finland, 70 lightning-caused failures of the main power transmission operator were reported in 2006. On the basis of the time of occurrence of the failures and the location information, the incidents were compared with the lightning first-stroke data available at FMI and found a DE of about 94% for the network.

OMSZ: the Országos Meteorológiai Szolgálat (OMSZ, national meteorological office of Hungary) is operating a SAFIR network consisting of seven sensors; five in Hungary and two in Slovakia.

RMI: the RMI has been operating a SAFIR lightning detection system (Systeme d'Alèrte Foudre par Interférométrie Radioélectrique) since August 1992. The sensors were provided by *Dimension* and are of type SAFIR-3000. The SAFIR network consists out of four stations with one in Dourbes, Oelegem, Jalhay (La Gileppe) and Mourcourt. Not long ago, one extra sensor is added at the RMI site in Ukkel which is currently semi-operational. Each sensor, being GPS synchronized, transmits in real time the data related to the specific event to a central processor. At present, the event location of lightning discharges is then determined by triangulation of the singals in the VHF band, after applying a least-square optimization algorithm (χ^2). The antennas are complemented with capacitive electrical antennas which allows discrimination between CC and CG.

At RMI the sensor data will be interpreted in the near future by the recently upgraded central processing system TLP230 of Vaisala, combining a VHF interferometric sensor (110–118 MHz) with a LF TOA sensor (300 Hz–3 MHz) for the localization and characterization of total lightning activity. It provides the user with specific functions related to the type of lightning sensor input data, i.e., low frequency (LF) or very high frequency (VHF). To ensure the data set applies to the same event, TLP230 collects lightning data from each sensor, compares the time at which the event was recorded by each sensor and then computes the lightning location. As such, TLP230 combines both LF and VHF data to develop location information from preliminary breakdown to ground strokes.

During the processes that create the channel, vast amounts of VHF radiation is emitted. Interferometric lightning location retrieval method for VHF signals is used to retrieve the location of the source. The VHF sensor records subsequently the event signal arrival time, signal am-

plitude, number of sensors participating in the lightning detection, and positional confidence (χ^2). But information about polarity is not provided. When high currents occur in previously established channels, i.e., the return stroke, the most powerful emissions occur in the LF range. In the LF, the radiation fields from CG strokes are strongest because of their channel length and large currents. Consequently, there are only a few pulses per flash. The LF sensors are capacitive electrical antennas which allow discrimination between CC and CG. For every LF event, the processed data includes sensor peak signal arrival time, peak field value, signal rise, signal decay time, as well as its polarity, multiplicity of the flash, number of sensors participating in the lightning detection, positional confidence (χ^2) based on the TOA method, maximum rate of rise of the waveform (kA/μs) and CG/CC discharge classification. The latter is done on the basis of the waveform of the signal detected by the capacitive antenna since, in contrary to CG discharges, CC discharges produce tens to hundreds of small pulses ($\sim$5% of the median amplitude of return strokes) in the LF range. Therefore, to disentangle the discharges into CG and CC, pulse shape and amplitude are considered, e.g., pulse rise time, peak-to-zero time, etc. However, despite the usefulness of these criteria a certain amount of pulses remain to be incorrectly identified. For instance, the lower the current, the more probable becomes misclassification of positive CC events as positive-polarity CG strokes (Orville et al. 2002). Moreover, Smith et al. (1999) and Jacobson et al. (2000) have found that distinct VHF radiation of CC processes is accompanied by VLF/LF emission with intensities varying from insignificant to very pronounced amounts, which exhibit feautures comparable to those of return stroke fields. This illustrates the need for effective procedures to distinguish between CC and CG discharges in VLF/LF observations. On the other hand, when a registered VHF source has no counterpart in the LF, it indicates that the source is a CC discharge. As such, TLP230 combines both LF and VHF data to develop location information from preliminary breakdown to ground strokes.

SHMU: the Slovenský HydroMeteorologický Ústav operates a SAFIR system consisting out three sensors in Slovakia. The data is combined with three more SAFIR sensors from Hungary.

SLDN: the Spanish Lightning Detection Network (SLDN) started in 1992 and currently operates more than thirty sensors in the LF region through magnetic direction finding and time-of-arrival combined detection techniques.

ZEUS: the ZEUS network, named after the mythological Greek God, is a long-range lightning detection network, operated by the National Observatory of Athens with six VLF receivers (7–15 kHz, centered at 9.8 kHz) located over Europe from 2001 onwards. The network uses the arrival time difference technique. ZEUS locating algorithm requires a minimum of four receivers to record the same event. ZEUS data has been compared to LINET data over a region limited to a part of Central-Western Europe (where LINET data exhibits the highest data quality) (Lagouvardos et al. 2009). It was found that the location accuracy is $\sim$7 km, while the detection efficiency was $\sim$25%. Therefore, ZEUS provides measurements that present a small location error, taking into account that it is a long-range detection system. Moreover, the analysis revealed that ZEUS is also capable to detect not only CG but also CC strokes, although with a decreased detection efficiency compared to CG strokes.

4.2   Some other large-scale networks in the world

LLDN: Vaisala's long-range lightning detection network (LLDN) sensors consist out of the (American) National Lightning Detection Network (NLDN), the Canadian Lightning Detection Network (CLDN) and the Pacific Lightning Detection Network (PacNet). The LLDN detection efficiency decreases with increasing distance from NLDN, CLDN and PacNet sensors. In addition, any long-range lightning detection network's DE varies as a function of time of day due to lightning signal propagation interaction with the ionosphere. Long-range lightning DE is higher during the night than during the day due to better ionospheric propagation conditions at night.

- *Canadian Lightning Detection Network* (CLDN): the primary design objective is to have a detection efficiency of >90% and a location accuracy of 500 m or better over those areas

of Canada having five thunderstorm days per year or more. The network consists of 51 Vaisala IMPACT LS7000 TOA sensors and 32 IMPACT ESP sensors.

The discharges detected by the CLDN are predominantly CG return strokes. Because the sensors are separated by 300–500 km, only a small percentage of cloud discharges are located by the CLDN. An analysis of the CLDN by Vaisala-GAI estimates that the flash detection efficiency is 85%–90% out to 200 km from the network periphery, decreasing to 80% at the periphery, and to 10–30% at a distance of 300 km beyond the periphery.

- *National Lightning Detection Network* (NLDN): the origin of the present NLDN configuration can be traced back to 1989 when the combination of three separate regional networks began real-time national coverage. Since then, a number of upgrades have been performed to increase the overall detection efficiency and location accuracy of the network. In short, in the early 1990s, the NLDN consisted of magnetic direction finding sensors with a DE of 65–80% and a LA of 2–4 km. The first major upgrade was completed in 1995 and included IMPACT Lightning Sensor technology, resulting in an increased flash detection efficiency of 80–90% and a 500 meter median location accuracy. This was followed up by a new upgrade in 2001 which replaced the old sensors with IMPACT ESP sensors and added 8 additional sensors which employ both electric and magnetic field sensing to provide both arrival time and azimuth information for each detected lightning discharge. At present the NLDN is a national network of 113 IMPACT ESP sensors that are placed 200–350 km apart. NLDN flash data provide time, location, polarity, amplitude and multiplicity of each CG lightning flash. Vaisala has estimated that the NLDN provides a CG flash detection efficiency that is better than 90% throughout the continental U.S. and that the DE for all CG strokes is in the range of 60–80% (Cramer et al. 2004). Note that the overall average DE for negative first-strokes is larger than the measured DE for subsequent-strokes that produce a new ground contact and the DE for subsequent-strokes that remain in a pre-existing channel. A median random position error of the NLDN was estimated to be ~400 m (Biagi et al. 2006).

- *North American Lightning Detection Network* (NALDN): in order to avoid boundary conditions between Canada and the US, CLDN and NLDN have been combined to form the North American Lightning Detection Network (NALDN), providing continental-scale coverage (Cummins 2000). The NALDN was developed to provide lightning information by accurately detecting and locating most cloud-to-ground (CG) lightning strokes and a small fraction of discharges produced by cloud flashes using magnetic field direction finding (MDF) and time-of-arrival (TOA) techniques. The NALDN allows lightning activity to be monitored in real-time for use in the protection of North American forests, for forensic applications such as in the electric power and insurance industries, and for a broad range of applications in weather nowcasting and climatology. The NALDN estimates the following information for each detected CG stroke: time, location, polarity, peak current and quality parameters related to location accuracy and consistency among reporting sensors. The flash detection efficiency ranges from 70% to 90% across Canada. The projected location accuracy indicates a median location accuracy of 500 m for the majority of Canada (Cramer et al. 2004).

- *Pacific Lightning Detection Network* (PacNet): its goal is to monitor lightning activity over the Central Eastern Pacific Ocean (north of the equator) with a network of ground-based lightning detectors being installed on four Pacific Islands[20] having distances between sensors of 400–3800 km. PacNet sensors are IMPACT-ESP sensors that combine both magnetic direction finding (MDF) and time-of-arrival (TOA) based technology to locate a strike with as few as two sensors. However, the location errors when only two sensors are used are somewhat larger when compared to locations produced by three or more sensors. These Pacific sensors work in combination with other sensors in the LLDN. The ~200 broadband LF/VLF sensors in these networks are not optimized for long-range detection but still provide important contributions to the overall network performance.

---

[20]The Islands in the North Pacific Ocean are: (i) Unalaska in the Aleutian Islands, Alaska; the Hawaiian Islands of (ii) Hawaii and (iii) Kauai; and (iv) Kwajalein in Marshall Islands.
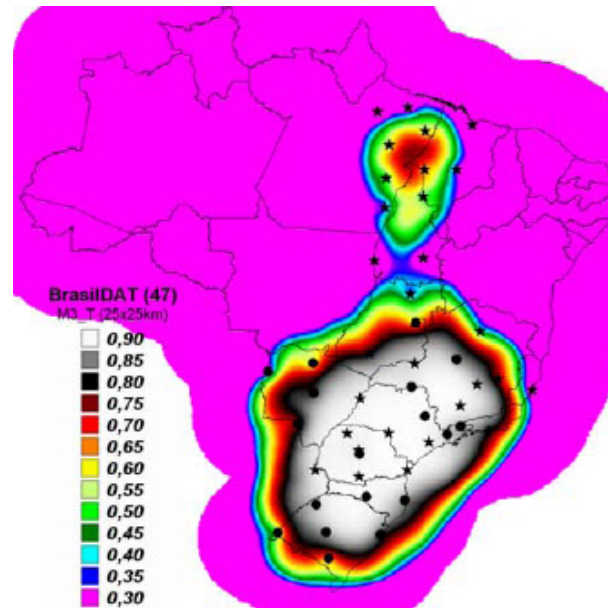
Figure 16: The computed BrasilDAT network detection efficiency.

The discharges detected by the PacNet/LLDN are predominantly CG return strokes, as CC discharges have typically weaker peak current than CG strokes and, as a result, remain below the detection threshold. The detection efficiency and location accuracy varies with time of day due to the diurnal changes in ionospheric electron density and ground conductivity. It is found that the DE is about 20% and 40% for day and night, respectively, with an observed location accuracy in the range of 13–40 km over the central North Pacific (Pessi et al. 2009).

As a result, PacNet/LLDN is one of the few observing systems, outside of geostationary satellites, that provides continuous real-time data concerning convective thunderstorms throughout a large area of the Pacific ocean. This is important since earlier on these remote regions did not have conventional data sources available. PacNet/LLDN data will therefore be able to provide real-time weather data to, e.g., naval aircraft carrier operations and civilian airports on the islands.

BrasilDAT: Brazil is the largest country in the tropical region of the world and has, estimated from total lightning observations by satellites and CG lightning observations by LLSs, the largest lightning activity in the world. Hence, studies on CG lightning in Brazil may lead to a better understanding of many aspects of the phenomenon, as well as the response of tropical lightning to different phenomena at many time scales.

The first LLS in Brazil operated in 1988, consisting of four LPATS sensors using TOA technology in the Southeast region of the country. Eight years later, the system was upgraded to include IMPACT sensors, combining MDF and TOA techniques. In 1999 this network was named Brazilian Integrated Lightning Detection Network (RINDAT). In 2006, two other networks began to operate in the North and South of Brazil consisting of ten IMPACT and 13 LPATS sensors, respectively. At present time, these different networks were combined to form the Brazilian Lightning Detection Network (BrasilDAT), which currently has 47 sensors installed of both LPATS and IMPACT type. More details about the BrasilDAT can be found in Pinto et al. (2006, 2007) and Pinto (2008). Nowadays, BrasilDAT is the third largest lightning detection network in the world.

Naccarato and Pinto (2008) presented a detection efficiency model (DEM) in which the peak current values and the distance of the CG lightning to the sensors are taken into account. This model also neglects the periods that each sensor is offline (due to communication problems) with a daily resolution. An example of the detection efficiency for the BrasilDAT network is plotted in Fig. 16. It is seen that the DEM indicates an average DE around 80% except in the North and Northeast regions of Brazil. The location accuracy, neglecting the regional
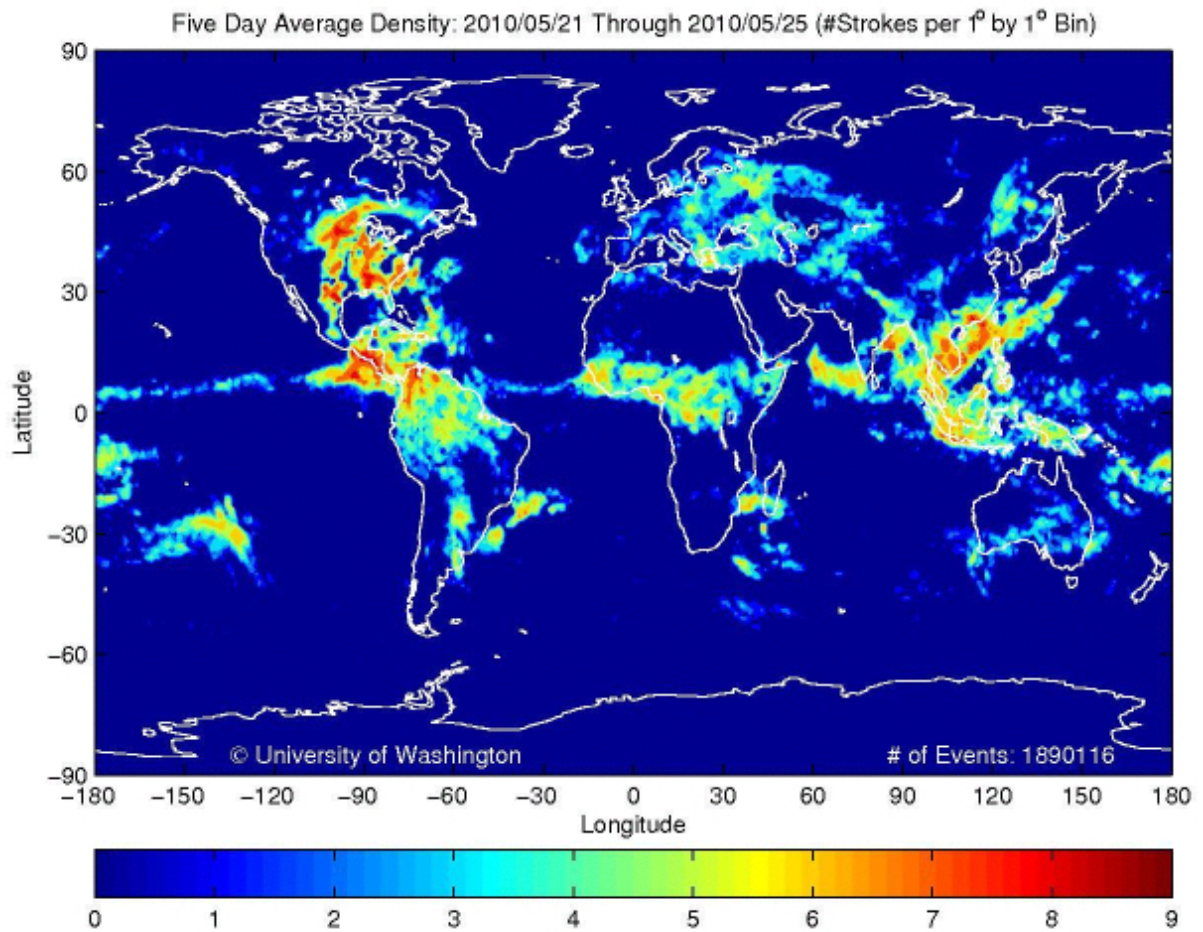
Figure 17: A five day average density image from the WWLLN network.

variations, is estimated to be $\sim 1\,$km.

WWLLN: an experimental very-low-frequency (VLF) World-Wide Lightning Location Network (WWLLN) has been developed through collaborations with various research institutes across the globe. At present 40 sensors in the network are active in detecting sferic activity (3–30 kHz) from lightning. These signals can be received thousands of kilometers from the source, as the electromagnetic radiation propagates its energy with low attenuation inside the waveguide formed by the conducting Earth and the lower boundary of the ionosphere, i.e., the Earth-Ionosphere Waveguide (EIWG).

The WWLLN makes use of a time-of-group-arrival (TOGA) algorithm to locate a lightning discharge, which compensates for the dispersion of the VLF sferic due to EIWG propagation. The ionospheric interaction spectrally distorts and attenuates the waveform leading to a dispersion of the initial sharp pulse of the lightning stroke into a wave train lasting a millisecond or more. The amplitude of the received sferic wave train rises slowly from the noise floor up, with no sharp onset and no sharply defined time-of-arrival (TOA) at the receiving station. The TOGA method makes a measurement of the time of group arrival from the progression of phase versus frequency using the whole waveform (Dowden et al. 2002). Using this method, the dispersion due to the VLF propagation is now less important, such that uncertainties in arrival times are now independent of the distribution of lightning source-receiver distances. TOGA measurements are grouped together such that for any given pair of TOGA measurements the difference in TOGA is less than the travel time between the two stations at which the measurements are made. Finally, using minimization methods, the lightning locations are determined.

The initial aim of the WWLLN is to provide real-time locations of cloud-to-ground and cloud discharges occuring anywhere on the globe, with a $>50\%$ flash DE and a mean LA of <10 km. The location accuracy and detection efficiency have been examined by contrasting its observations with those from other detection networks in Australia, Brazil, America and New Zealand (see Lay et al. 2004; Jacobson et al. 2006; Rodger et al. 2005; Rodger et al. 2006). It was found that the WWLLN detects both CG and CC lightning strokes, although due to the higher peak currents in CG strokes, the network is better suited for detecting CG strokes. The DE of $\sim3\%$ is rather low and the WWLN has a spatial accuracy of about 15 km. However, for many scientific applications, the benefits of a global overview in real time can outweigh the very low total lightning detection. For instance, WWLLN activity maps have been used to deliver information on where the most lightning-active thunderstorms are located to observe from space the production of red sprites (Yair et al. 2004). Note that with an increase in active sensor spread around the world the aforementioned values of DE and LA may eventually reach its initial goal.

5 Scientific exploitation of the data

Extreme weather is a major hazard all over the world, often accompanied by violent natural disasters such as hail and wind storms, tornados, flash floods, forest fires and lightning damages. In addition to the number of lightning discharges, lightning detection sensors can also provide information on lightning characteristics such as the ratio between intra-cloud and cloud-to-cloud lightning, the polarity of the discharge, peak currents, etc. which is of strong scientific interest. The importance of these studies is further strengthened by the fact that it not only can be used by physicists trying to understand lightning phenomena, but also by meteorologists who can possibly use lightning information in climate change and severe weather studies, and by engineers wanting to protect electrical and electronic systems from the deleterious effects of lightning.

In this chapter we start with some brief characteristics of thunderstorms, followed by an overview of the different aspects in which lightning detection data can be used for scientific purposes. Note that it is not the intention of the author to be complete, nor is it feasible. As such, it is merely to provide the reader with an idea of some possibilities for which lightning data can be used and to show the necessity to conduct lightning research at a meteorological institute.

5.1 Characteristics of storms indicative of lightning production

Prior to the development of automatic lightning detection systems, the only means for identifying thunderstorms was to infer their existence from measurements of the storm characteristics. In the following we discuss briefly some of these characteristics that can give the observer a somewhat better idea whether a cloud will produce lightning or not. However, it must be kept in mind that storm electrification requires complicated interactions, as seen in Sect. 1.3 and following. Therefore, it is not straightforward for a simple parameter test to have a high degree of diagnostic skill. In this section, in contrary to following sections, no attempts have been made to distinguish between positive and negative CG lightning.

(i) *Radar reflectivity*: is a straightforward test to determine if a cloud is a thunderstorm by using a certain threshold on the maximum reflectivity found in a storm during a radar scan. One threshold used in the past in meteorological operations has been that storms having a reflectivity of at least ± 40 dBZ are thunderstorms. However, it is obvious that the extent to which this rule is valid varies from region to region, and from one event to another.

A general trend has been observed in that the probability of producing ground flashes rises with increasing reflectivity (Reap & MacGorman 1989), but is never 100%. Furthermore, only 50% of the observed storms having a reflectivity > 40 dBZ produce ground flashes.

(ii) *Cloud top temperature and storm height*: several studies have noted that lightning activity begins when the top of the radar echo of the storm grows to an altitude where the temperature is $\leq$ -20°C (e.g., Lhermitte & Krehbiel 1979). However, the use of one specific threshold leads to either an inadequate probability of detection or to false detection of some non-thunderstorm clouds as thunderstorms. This can be seen in the observations of Jones (1950) who found that the probability of lightning increased with decreasing cloud top temperature for cloud tops colder than -25°C, i.e., for taller clouds, but also observed several storms with cloud tops between -25°C and -40°C that produced no lightning at all.

Holle & Maier (1982) examined the probability of ground flashes produced as a function of the altitude of the radar-determined storm top for storms in Florida and found that the minimum height at which ground flashes occur was 7.8 km, with a median temperature of -18°C isotherm. The probability of a storm producing ground flashes was less than 100% until the altitude of the storm tops reached 16 km. The increasing probability of lightning occurrence with increasing storm height can be explained by the trend that the electric field tends to increase inside thunderstorms as the storm height increases (Mach & Knupp 1993).

(iii) *Convective growth*: one reason that a specific threshold for the height can be misleading in identifying storms as thunderstorms is that tall storms can have updrafts with insufficient speed or spatial extent to drive electrification mechanisms triggering lightning. Workman & Reynolds (1949) were some of the first to show that the amount of lightning produced by a thunderstorm is closely tied to the updraft evolution and appearance of an ice phase. Later on, it has been suggested that the presence of powerful convective growth at temperatures between -10°C and -20°C is a prerequisite for lightning; the region where the non-inductive mechanism, as discussed in Sect. 1.3, is effective. This is because strong vertical velocities in the mixed-phase region enhances the non-inductive electrification mechanism by providing vast amounts of large ice particles and sufficient concentrations of supercooled liquid water. For example, Lhermitte & Krehbiel (1979) observed a pronounced increase in flash rates when there is an increase in the rate of cloud height growth and an increase in updraft speed to $>20\,\mathrm{m\,s}^{-1}$ at temperatures colder than -10°C.

It is worth mentioning that Météo-France has developed a Rapid Development Thunderstorm (RDT) product in the framework of the EUMETSAT Satellite Application Facility (SAF) in support to nowcasting and very short range forecasting. With the use of predominantly geostationnary satellite data, it is possible to identify, monitor and track intense convective system clouds, as well as to detect rapidly developing convective cells.

5.2 Comparison of radar precipitation fields with lightning observations

Experimental studies show that environmental conditions, i.e., temperature, dynamics and microphysics within a storm, play a major role in the lightning-rainfall connection. This is true as the strength of the updraft and the vertical distribution of the temperature control the vertical distribution of hydrometeors. This results in a different interaction between ice particles and supercooled water, leading to a different charge separation influencing the lightning activity (e.g., Williams 1985; Chauzy et al. 1985; Michimoto 1993; Soula et al. 1995). In the same way, the occurrence of flashes largely differs between continental and oceanic storms, due to the difference in convective intensity (Rutledge et al. 1992; Williams et al. 1992). The rain-yield per flash is much larger in oceanic convective clouds, due to the weakness of the updrafts over the ocean compared to over land. In addition, the lightning density can be larger by three orders of magnitude over land than over ocean at the same latitude. In ocean storms, the width and the height of the mixed-phase cloud region, where the non-inductive charging processes occur, are often too small for the development of electrification. Zipser (1994) examined variations in the Rain-to-Thunder days Ratio (RTR) calculated from monthly quantities. He showed that RTR values for areas over oceans were substantially higher than those for areas over land. All in all, these results indicate that climatic parameters influence the lightning-rainfall relation.

According to several studies in which rain and lightning activities are observed simultaneously, a tight relationship is found (Battan 1965; Kinzer 1974; Piepgrass et al. 1982); an increase in rain generally corresponds with an increase in CG flash rate. Quantitative estimates of the water volume per CG flash have been made, which depends very much on the thunderstorm type and region, with values ranging from $30\times10^3\,\mathrm{m}^3$/CG flash to $1000\times10^3\,\mathrm{m}^3$/CG flash. This variation has been attributed to various causes in the literature, according to the techniques of rainfall estimation, the region of the storm activity, the type and phase of the storms involved, and the type of flash considered. More detailed relationships can be found with respect to the characteristics of the lightning activity in terms of CG positive proportion or CC activity (Soula & Chauzy 2001). It is found that positive CG flashes are associated with higher rainwater volume than negative flashes. By introducing a weight coefficient for positive CG flashes, Soula & Chauzy (2001) find that taking into account a specific contribution of each type of lightning flash, the amount of rain can be estimated from the total electrical activity of the system, with good comparison to radar measurements. However, it is worth noting that in these studies a positive CG with low peak current ($<10\,\mathrm{kA}$) can be misindentified as an intra-cloud lightning flash (Cummins et al. 1998; Orville & Huffines 2001; Carey et al. 2003).

Another type of correlation is the spatial correspondence between rain and lightning flashes.

According to several authors, the flash activity core does not correspond to that of precipitation (e.g., Carte & Kidder 1977) and lightning flashes tend to strike just outside the region of highest reflectivity (Lopez et al. 1990). This could be explained by the fact that in the mature stage of a thunderstorm, areas experiencing a downward cool flow with precipitation and areas with an upward warm flow, i.e., areas favorable for the onset of electrification processes, do not occur at the same place when a vertical wind shear is present. On the other hand, in some cases these cores do correspond (Kuettner 1950; Soula et al. 1998), due to the lack of a vertical wind shear. In addition, Pineda et al. (2006) analyzed the relationship between precipitation and lightning in the North Western Mediterranean coast and found that lightning activity is not restricted to the highest rainfall areas, but spreads to zones with lower rainfall accumulations. The lightning locations in the latter study were reported with the use of the Meteocat SAFIR lightning detection system, having a location accuracy of around 2–3 km (Montanyà et al. 2006).

Furthermore, it has been observed that heavy gushes of rain shortly follow a lightning flash. For instance, Moore & Vonnegut (1977) showed that 75% of summertime precipitation that had fallen on one mountain top station has done so within 5 min of a nearby lightning discharge. In addition, positive time lags between the peaks of flash rate and rain intensity at the surface have been shown by many other authors, e.g., Piepgrass et al. (1982), Ćurić & Vuković (1991). Although from these observations the close association between lightning and precipitation is evident, there is still no agreement about the mechanism operating in thunderclouds. Two main different mechanisms have been proposed to explain how lightning might cause the formation of a rain gush: one is acoustic and the other is electric. Goyer (1965a,b) experimentally showed that rain gush is the result of an increased rate of coalesence between water droplets due to the radial wind produced by the explosion following a lightning discharge. However, according to Vonnegut & Moore (1960) lightning introduces electric charges that accelerate the coalescence of cloud droplets. Likely, a combination of the two mechanisms is responsible for the observed phenomenon.

5.3   Relationship between lightning type and convective state of the thundercloud

Some researchers have focused on the phenomenon of predominantly positive CG producing (PPCG) storms. By definition, at least 50% of the CG lightning in PPCG storms is of positive polarity. PPCG storms are often severe (producing hail, damaging winds, or tornados), and can have a high amount of CC flashes. In contrary to PPCG storms, low-CG storms experience (as the name suggests) very little CG lightning (often $<1\,min^{-1}$ and sometimes no CGs for more than 10 min) and large CC flash rates. The question asked is what distinguishes low-CG from PPCG storms? One approach to address this question is by looking at the possible kinematic, microphysical and environmental differences between these storms. MacGorman et al. (1989) suggested that low-CG storms might be caused by an *elevated charge mechanism*, where intense updrafts loft the main negative charge layer to greater altitudes than normal. Thus, the reduced electric field between the main negative charge and ground due to the greater spatial separation results in a reduction in CG lightning flash rate. However, the total lightning flash rate increases due to stronger charging driven by the intense updrafts in combination with less separation between the main negative charge layer and upper positive layer. In addition, three mechanisms are proposed to explain the PPCG behaviour: (i) the *tilted dipole* mechanism (MacGorman & Nielsen 1991, Branick & Doswell 1991) posits that upper positive charge is displaced laterally by strong upper-level winds, thereby unshielding it from the negative charge below and exposing the positive charge to the ground. (ii) The *inverted dipole* mechanism (MacGorman & Nielsen 1991; Williams et al. 1991) suggests that in PPCG storms the lower positive charge layer may become dominant, causing the classical dipole to invert. The lower positive charge would favor positive instead of negative CGs. (iii) The *precipitation unshielding* mechanism (Carey & Rutledge 1998) suggests that in intense storms the precipitation mass flux becomes sufficiently large such that the negative charge center is effectively removed (or greatly reduced) by the fallout of precipitation particles. The unshielding and exposing of the

upper positive charge causes positive CG flash rates to increase.

Lang & Rutledge (2002) examined lightning observations of 11 thunderstorms. In their analysis, a kinematic intensity (KI) index of the individual thunderstorms has been quantified, based on the peak vertical velocity, the volume occupied by significant updrafts within the mixed-phase region and the vertical airmass flux. They find – even though the small sample size – a tendency for storms with a moderate intensity range to exhibit greater negative CG flash rates compared to storms with large KI; behavior consistent with the elevated charge mechanism. On the other hand, storms with large KI tend to produce high values of positive CG flash rates, opposed to low values for low KI thunderstorms. In addition they find that positive CG lightning peaked as the rain and hail production increased significantly. This is broadly consistent with the precipitation-unshielding mechanism. Overall, the evidence for any specific PPCG mechanism from their dataset appears ambiguous and it is entirely possible that multiple processes are active at once. It is important to emphasize that the correlation between positive ground flashes and severe weather appears to be valid in only one direction. Although storms with frequent positive flashes appear likely to produce severe weather, severe weather also occurs in the much more common storms dominated by negative ground flashes (e.g., Doswell & Brooks 1993; MacGorman & Burgess 1994; Perez et al. 1997; Galarneau et al. 2000). However, storms dominated by frequent positive ground flashes for a period of time appear to produce severe weather in all or most cases, whereas only a relatively small fraction of storms dominated by negative flashes experiences severe weather.

5.4   Temporal and spatial relations between hail and lightning

Besides hailstones, hailstorms usually produce heavy rain, gusts and lightning, which may destroy crops, houses, cars, etc. Many studies of lightning characteristics in hailstorms have been conducted since the 1980s. Delobbe et al. (2004) found a positive correlation between the location of high probability of hail versus the electrical activity, with larger hail sizes being associated with higher electrical activity. Rust et al. (1985) and Reap & MacGorman (1989) analyzed the relationship between CG lightning activity and hailfall and found that large hail is more likely to occur in storms that have high densities of positive CG flashes. Changnon (1992) noticed from observations of hail streaks in Illinois that negative CG flash rates typically increased until hail damage began, decreased (but remained large) during damage and decreased more rapidly after hail damage ceased. In supercell storms examined by MacGorman & Burgess (1994) large hail was reported during periods when positive CG flashes dominated and a decrease of hailstone diameters was noticed after dominant positive polarity switched to negative. Williams et al. (1999) investigated CG flash activity of severe Florida thunderstorms and observed abrupt increases in flash rates 5–20 min prior to microburst and hailfall occurrence and peaked at hail initiation. After the hail ended, the flashes diminished and typically ended 10 min thereafter. Carey et al. (2003) showed that the distribution of positive CG storms varied geographically and by month. Both Carey et al. (2003) and Carey & Buffalo (2007) noticed that the occurrence of positive CG storms were associated with specific properties of the meteorological environment. Temporal and spatial factors may influence the behavior of CG lightning activity in relation to hailfall, which is thought to be the result of differences in dynamical and microphysical processes in severe thunderstorm clouds. This was also indicated by Williams (2001) in a conclusion of his review on this topic by stating that "the examination of individual cases emphasizes a large variability". However, a general trend is observed in that positive CG flashes dominate for most of the lifecycle in hailstorms, while negative CG flashes are typically inactive. A rapid increase of the CG flash rate might indicate the occurrence of hail falling. In the termination stage, the CG flash rate decreases gradually, but the proportion of positive CG flashes can still be large. Note that CG rates corresponding to hail-bearing storms/thundercells is typically a factor of 5 lower than those of rain-only storms. The evolution of CG flashes for a hailstorm in northern China is shown in Fig. 18 (Liu et al. 2006).

To explain the positive polarity of CG flashes dominating in most of the hailstorm lifecycle, two possible reasons can be proposed. (i) The first one is that it could be related to the inverted
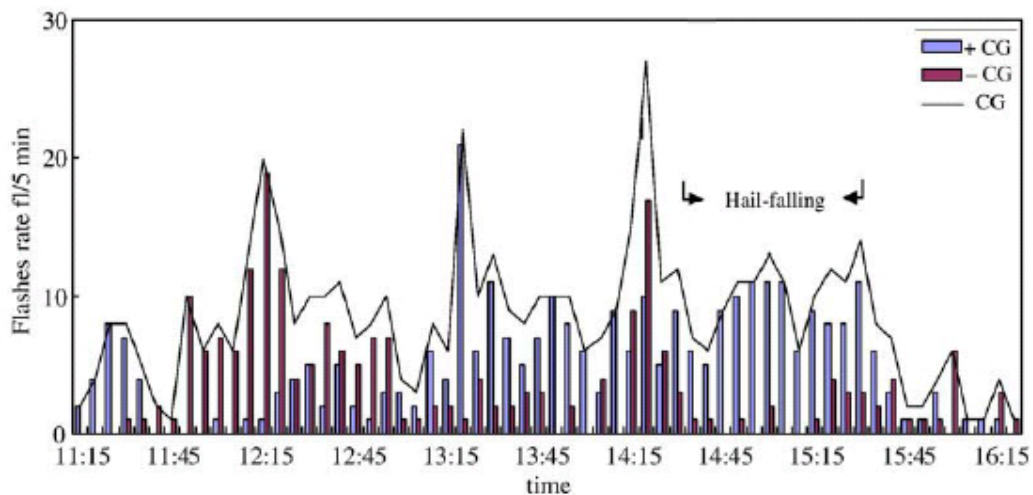
Figure 18: Flash rate evolution of CG flashes for a hailstorm in northern China. It is seen that the period of falling hail corresponds to the stage of active positive CG flashes. A peak in CG flash rate occured at 1425 UTC, 10 min prior to the beginning of the hail-falling. A possible reason is that the charging could be enhanced with the ice particles increasing in the cloud, resulting in a quick increase of CG flash rate. It is hypothesized that the decrease in the number of ice particles at the beginning of hail-falling weakened the electrification in the cloud, which resulted in a rapid decrease of negative CG flashes.

charge structure in the hailstorm. In some thunderstorms or in some stages of the storm there could exist an inverse charge structure contrary to the normal polarity, i.e., the major positive charge is in the middle-level and negative charges in the upper-level. (ii) The other possibility could be related to an inclined dipole charge structure resulting from the wind shear effect.

Chagnon (1992) addressed the positional relationship between hail and CG flashes and found that the most common positions with respect to the hailstreaks of the lightning centers was parallel and along the left flank (44%) of the streak, with the next most common position (22%) along the right flank. The key finding is that CG lightning associated with hail almost totally occurs close to but beyond the hail shaft.

In many of the above studies mentioned, no information about intra-cloud lightning activity was available and therefore one needs to be careful when drawing conclusions w.r.t. the characteristics of lightning in hailstorms. Therefore, to improve further our understanding of the charge structure and discharge characteristics of hailstorms one needs to accumulate total lightning measurements (CC + CG), as intracloud flashes can be in very large proportion and may precede the CG activity. This, in combination with numerical simulations of the relationships among the microphysical, dynamical and electrification processes in hailstorms, will strengthen the general features of lightning activity observed in hailstorms.

5.5 Cloud-to-ground versus intracloud lightning

Convective storms are well recognized to produce two common types of lightning: intracloud (CC) and cloud-to-ground (CG). Already early in the studies of lightning it was clear that CC lightning precedes during the upward development of convective clouds. This conclusion was drawn by observing thunderstorms in New Mexico (Workman & Reynolds, 1949). A typical time difference between the initial preceding CC flash and the initial subsequent CG flash was 6 min. Many studies have followed to examin the CC-CG relation. Lhermitte & Krehbiel (1979) for instance found that as many as 15 CC flashes precede the first CG flash in the initial stage of a storm. In a later, more vigorous, stage of the convective development, CC lightning rises in parallel with the vertical development. Additionally, it was observed that the later onset of CG lightning was well correlated with the initial descent of the 55 dBZ reflectivity core beneath the level of main negative charge. MacGorman et al. (1986) have investigated CC and CG lightning in substantially larger storms which exhibited a mesocyclone and tornado. The CC
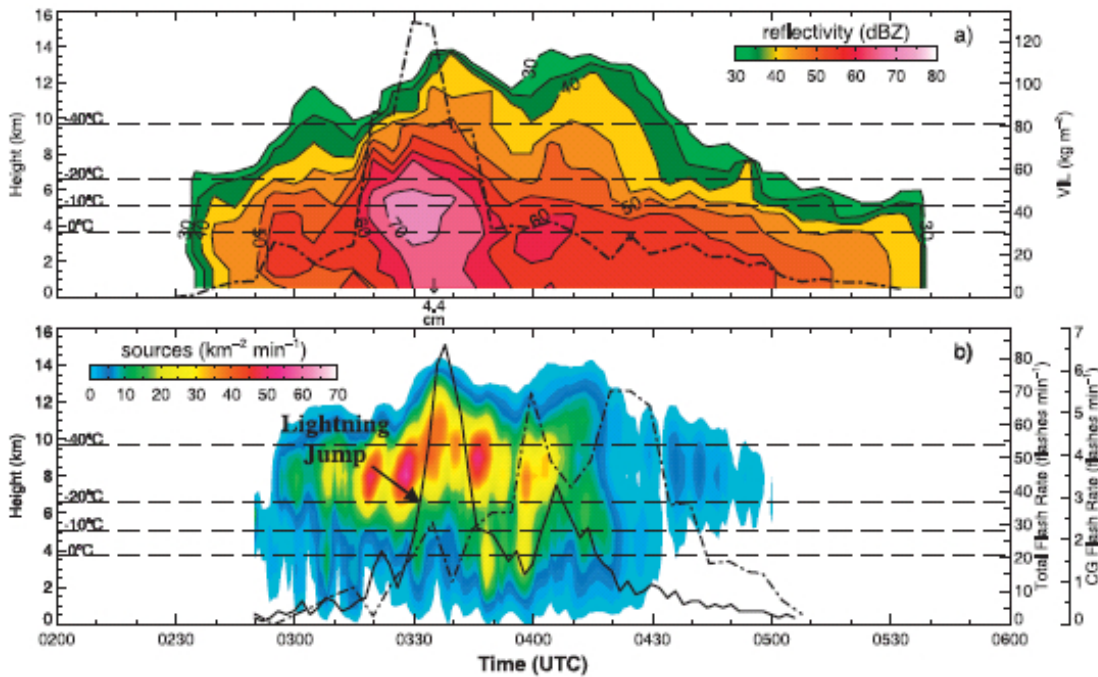
Figure 19: Time-height evolution of (a) radar reflectivity (contours) with VIL (dash-dot line) and temperature (dashed lines). (b) VHF source density (contours) with 2-min total flash rate (i.e., flash rate averaged over a 2-min period; solid line) and 5-min CG flash rate (i.e., flash rate averaged over 5-min period; dash-dot line) from a nontornadic hail-producing thunderstorm on 30 Mar 2002. From Gatlin and Goodman (2010).

lightning activity was associated with the period of greatest vertical development in which all the particles (ice crystals, supercooled droplets, and graupel) are moving upward relative to the ground. The later decline in CC activity is accompanied by an increase in CG activity, when the ice particles begin to descend. The analysis of radar reflectivity evolution at various heights suggests that large quantities of ice are descending at levels at and below the height of the main negative charge during the period of predominant CG activity. Both laboratory (e.g., Takahashi 1978; Jayaratne et al. 1983; Illingworth 1985) and field measurements (e.g., Marshall & Winn 1982) suggest that graupel particles will acquire positive charge at levels beneath the main negative charge, which may promote CG lightning.

To summarise: observations show that (i) CC lightning dominates in the early stages and is well correlated with the upward development of the cloud, the growth of ice particles, and radar reflectivity above the inferred negative charge region. Ten or more CC flashes may occur before the first CG event. (ii) CG lightning activity (less frequent than CC) lags the initial CC peak by 5–10 min (e.g., Carey & Rutledge 1996). The initial CG activity is associated with the descent of precipitation particles (hail and graupel). These observations can be linked to physical processes in the various stages of a thundercloud: (1) The CC lightning is the result of charge separation by ice particle collisions and differential motions in the upper region. Negative charge is selectively charged to larger particles in this region. (2) While negative charge accumulates at midlevels, it may not be energetically favorable to transfer negative charge to ground in CG lightning. The analysis of radar reflectivity evolution at various heights suggests that the cloud-to-ground lightning may be stimulated by the subsequent descent of ice particles through the level of the main negative charge and the action of charge reversal microphysics which endows the larger ice particles with positive charge. It is believed that the increase of lower positive charge allows for negative charge transfer to ground in CG lightning. An example of the time-height evolution of radar reflectivity and electrical activity is plotted in Fig. 19.

5.6 Lightning data to improve nowcasting

With the advent of lightning data for operational use in the nowcasting of thunderstorms – in particular severe thunderstorms – the understanding of how microphysical and dynamical processes affect lightning production, including flash rate, type and polarity, etc. may provide better insights into short-term prediction of severe weather, such as large hail and floods. These questions are difficult to answer as there is a variety of convective storm types, as well as different lightning patterns, manifested in cloud-to-ground lightning flash rates, dominant polarity of cloud-to-ground lightning, total and intracloud lightning flash rates, the ratio of intracloud to cloud-to-ground lightning and so on.

Previous sections in this chapter were attributed to studies that tried to link lightning characteristics to certain weather patterns. One of these analysis found a possible relationship between storm severity and predominantly positive cloud-to-ground (PPCG) lightning activity, suggesting that real-time lightning data may be useful in the nowcasting of some severe local storms (Lang & Rutledge 2002). However, as pointed out by Branick & Doswell (1992), "before we can use lightning polarity data effectively in warning operations, we must learn why only some severe storms produce high positive CG rates, and, in particular, *which* storms." On the other hand, Hohl & Schiesser (2000) examined relationships between radar-derived hail kinetic energy and cloud-to-ground lightning stroke rates and found that negative CG stroke rates are in good linear correspondance with total amounts of hail kinetic energy[21], whereas totals of positive CG stroke rates are in no direct correspondence with $E_{kin,tot}$. The study suggests that negative CG stroke rates could be used to support and improve nowcasting operations for severe hailstorms.

Contrary to studies which use only one particular CG lightning type (positive or negative), are those which use total lightning activity to help to diagnose the severe weather potential of a thunderstorm. Only recently has there been an algorithm that provides an early indication of impending severe weather from observed trends in thunderstorm total lightning flash rates (see Gatlin & Goodman 2010). This algorithm is based upon the observations of rapid increases of total lightning activity preceding severe and tornadic thunderstorms (Williams et al. 1999; Goodman et al. 2005), by typically 5–25 min. The term *lightning jumps*, to denote the rapid increase in total flash rates, has been first proposed by Williams et al. (1999), and are characterized by a rapid increase in total lightning activity followed by a relative maximum and ends with a slow decline in lightning activity. As mentioned in Sect. 5.1, several studies indicate that strong updraft triggers lightning production. This updraft provides water vapor into the cloud which leads to more condensation and hence a higher concentration of graupel-sized ice particles. As more and more ice particles collide with each other, an electrical charge within the cloud is build up as the updraft separates the charge, thereby leading to an increase of intracloud lightning activity. Eventually the graupel grows large enough to fall from the updraft towards the ground, resulting in fewer intracloud lightning flashes. Hence, lightning jump identification within thunderstorms can be used to predict severe weather events. However, it was found that not all severe weather is preceded by a lightning jump, nor do all storms that produce these rapid increases in lightning contain severe weather. The performance of the lightning jump algorithm as described in Gatlin & Goodman (2010) showed the potential of this technique with a satisfactory DE of 0.75–0.9 and a FAR of 0.34–0.6, depending on different configurations of the algorithm. In order to further increase the performance of a warning system for severe weather events, algorithms using the total flash rate evolution as described earlier need to be linked with for instance cloud-top height data from satellite observations.

---

[21] The hail kinetic energy is calculated from CAPPI reflectivities, using the relation between the radar reflectivity factor Z and the vertical flux of the kinetic energy $\dot{E}$ given in Waldvogel et al. (1978) as: $\dot{E}=5\times10^{-6}\times Z^{0.84}(\text{Jm}^{-2}\text{s}^{-1})$. To obtain the entire hail kinetic energy, the flux $\dot{E}$ is integrated over the considered time interval and the area with reflectivities indicating a hail signal, i.e., $E_{kin,tot} = \int_{t_0}^{t_1}\int_{s_0}^{s_1}\dot{E}(x,y,t)\mathrm{d}x\mathrm{d}y\mathrm{d}t$.

6 Conclusions & future prospects

We have given an overview of the different physical aspects involved in the formation of lightning discharges, focussing in particular on the downward negative discharge to ground as it is the most common and studied type of cloud-to-ground lightning. It is clear that even though the electric characteristics in the atmosphere have been studied for centuries now, grey areas in lightning research still exist. On one hand, this is particularly apparent for instance in the field concerning the mechanisms responsible for the electrification within thunderclouds or the initiation of a lightning discharge, i.e., to what extent are cosmic-ray collisions with atoms and molecules responsible for the onset of lightning? On the other hand, new territories are opened with the advent of recently discovered exotic lightning discharge types such as blue jets, sprites and elves. As such, current theories need to be adapted or even rewritten. Moreover, studies have shown that the distribution of lightning around the Earth is directly linked to the Earth's climate driven by the solar energy. This seems to be true, although different theoretical models do not agree with each other whether a warmer climate in the future would produce now more or less lightning for every degree of global warming. In addition, the impact of lightning on air chemistry cannot be underestimated as the discharges produce vast amounts of nitrogen oxide NO_x facilitating chemical reactions in the troposphere and stratosphere which in their turn determine the concentrations of ozone O_3. Note that these chemical changes in coicidence with lightning can be measured with for instance the SEVIRI instrument on Meteosat's second generation satellite, as well as with the MIPAS spectrometer onboard the Envisat satellite. As such, a clear understanding of the phenomenon not only helps to apprehend the full picture locally, but also on a global scale. Undoubtedly, laboratory experiments that closely replicate the conditions prevailing in thunderstorms are a neccesity to address these open questions as well as more observations of the different phenomena in thunderstorms to uncover step by step the beauty of this extraordinary eyecatcher.

Lightning detection and location principles are in use for some decades now. The most commonly used lightning location systems (LLS) are based on interferometry, magnetic direction finding and time-of-arrival techniques or a combination of them. Each specific (ground-based) lightning location system uses a unique sensor configuration. However, the main difference between the various operational LLS is in the used detection frequency of the sensors, i.e., (very)-low-frequency (VLF/LF) versus very-high-frequency (VHF); tailored to the needs and requirements of the end user, e.g., aviation security, power utilities, insurance companies, or scientific purposes. Networks operating in the LF or VHF range do not reach presently far enough to cover oceanic or other remote areas, as large attenuation of the signals at these frequencies prevent the observation of lightning discharges at large distances. As such, no lightning data is provided over large parts of the tropics (Africa, Asia) and other isolated territories, as well as over the oceans by sensors operating in this waveband. Luckily, VLF networks come to help as signals at these frequencies can travel relatively with low attenuation over large distances via the Earth-ionospheric waveguide (EIWG). In addition, existing satellite based lightning detection sensors routinely detect lightning and give reliable data, however with restricted temporal coverage over a particular area. In the past years, much experience have been gathered in the processing, validation and application of the data. The reliability and quality of the data, related to the detection efficiency (DE), location accuracy (LA) and false alarm rate (FAR), differs between the existing operational LLS. In general, VHF/LF networks produce more precise lightning data then networks based on VLF signals. However, both type of systems deliver a wealth of data concerning the processes governing lightning production, local flash characteristics as well as global behavior. It is clear that to advance our knowledge of lightning, more accurate lightning data is needed on local and global scales. Therefore, it is important for every LLS to make regularly improvements in order to alter the quality and availability of the data.

The RMI of Belgium started some 15 years ago with an operational LLS. Recently, the network has been updated with a new TLP230 central processor. The LLS is able to locate CG as well as CC lightning discharges. Since lightning data can/will be used for a multitude of applications, including the continuous monitoring of thunderstorm activity, nowcasting of severe weather, etc., the knowledge of the capabilities and the measurement limitations of the lightning de-

tection system are considered particularly important. Hence, the first key task at RMI will be the verification of the current lightning detection system, i.e., estimation of the DE, LA, and FAR, and to try to boost the quality of the lightning observations. For this, lightning data from previous years obtained at RMI will be correlated with data from other lightning detection systems, e.g., ATDNET, LINET. In addition, lightning data will be validated against observed ground truth, e.g., railway and power plant damage reports. Once the quality of the data has been assessed scientific studies can be executed.

Research projects will include the improvement of the information provided by the climatological service based on quality-controlled lightning observations. Produce of meta-data on the quality of lightning observations for an optimal use by the climatological service. Improved nowcasting of thunderstorms through an optimal integration of real-time lightning observations, and improved warning for lightning strokes, i.e., integration of lightning observations in the operational nowcasting tool which is currently under development. Finally, further development (refinement) of the lightning warning system (SAFIR sms) is envisaged.

Finally, for more in depth information related to the topics addressed in this manuscript, I refer the interested reader to various textbooks on atmospheric electricity by MacGorman & Rust (1998), Rakov & Uman (2003) and Uman (1984).

List of acronyms

ATDNET	Arrival Time Difference NETwork	
	Lightning detection system operated by the United Kingdom Met Office	
BJ	Blue Jet	
	Slow moving fountains of blue light from the top of the cloud of active thunderclouds	
CC	Cloud-to-Cloud	
	Lightning discharges that do not involve contact with ground	
CG	Cloud-to-Ground	
	Lightning discharges that effectively lower charge to ground	
CRI	Cosmic Ray Intensity	
	Denotes the intensity of cosmic rays penetrating the Earth's atmosphere	
DE	Detection Efficiency	
	The ratio of the number of detected events divided by the real number of events that actually occured	
DMSP	Defense Meteorological Satellite Program	
	The DMSP designs, builds, launches, and maintains satellites monitoring the meteorological, oceanographic, and solar-terrestrial physics environments	
EIWG	Earth-Ionosphere WaveGuide	
	Waveguide formed by the conducting Earth and the lower boundary of the ionosphere	
ELF	Extremely Low Frequency	
	Is a term used to describe radiation frequencies from 3 to 30 Hz	
EMP	Electromagnetic Pulse	
	A high-intensity, relatively short-duration burst of electromagnetic energy	
EUCLID	EUropean Cooperation for LIghtning Detection	
	Is a collaboration among national lightning detection networks with the aim to identify and detect lightning all over the European area	
FAR	False Alarm Rate	
	Is the partition of wrongly detected non-lightning events	
GEC	Global Electric Circuit	
	Is a concept that links the electric field and current flowing in the lower atmosphere, ionosphere and magnetosphere	
IC	Intracloud	
	Discharges occuring between a thundercloud	
IMPACT (-ESP)	Improved Performance from Combined Technology (-Enhanced Sensitivity and Performance)	
	Type of lightning detecting sensor combining the magnetic direction finding (MDF) and time-of-arrival (TOA) technique to determine a location of the signal	
KI	Kinematic Index	
	Used to quantify the intensity of a storm based on the vertical velocity, volume of updrafts and the vertical airmass flux	
LA	Location Accuracy	
	Is a measure of how well the location of an individual lightning discharge is determined	
LCL	Lifting Condensation level	
	Is the height above which a parcel of warm, moist air starts to condense	
LF	Low Frequency	
	Is a term used to describe radiation frequencies from 30 to 300 kHz	
LI	Lightning Imager	
	An instrument on future satellites to observe the lightning activity and provide lightning locations	

LLS   Lightning Location System
A network of lightning sensors that work together to observe lightning discharges

LPATS   Lightning Positioning and Tracking System
Type of sensor that uses the time-of-arrival (TOA) method for position retrieval

MDF   Magnetic field Direction Finding
A method to determine the location of a lightning event based on magnetic field changes

PLD   Positive Lightning Discharge
Those flashes that transport positive charge from cloud to the Earth's surface

PPCG   Predominantly Positive CG (producing storm)
By definition, at least 50% of the CG lightning is of positive polarity in a PPCG storm

RDE   Relative Detection Efficiency
The RDE of a sensor is the ratio between the number of CG flashes reported by the sensor and the total number of CG flashes detected by the network

RDT   Rapid Development Thunderstorm
A tool developed by Météo-France making it possible to nowcast and provide very short range forecasting

RS   Return Stroke
The intense luminosity that propagates upward from Earth to cloud base in the last phase of each lightning stroke of a cloud-to-ground discharge

RTR   Rain-to-Thunder (days)
An RTR ratio divides the rainfall by the number of thunder days

SL   Stepped Leader
The initial leader of a lightning discharge; an intermittently advancing column of high ionization and charge that establishes the channel for a first return stroke

SR   Schumann Resonance
Are a set of spectrum peaks in the extremely-low-frequency (ELF) portion of the Earth's electromagnetic field spectrum

SAFIR   Surveillance des orages et Alerte Foudre par Interférométrie Radioélectrique
A SAFIR system detects the lightning discharges with the interferometric method

TLE   Transient Luminous Event
The collective name given to a wide variety of optical emissions which occur in the upper atmosphere above active thunderstorms

TOA   Time of Arrival
This technique use the the arrival times of the impulsive emission at a number of antennas to determine the location of the discharge

VHF   Very High Frequency
Is a term used to describe radiation frequencies from 30 to 300 MHz

VLF   Very Low Frequency
Is a term used to describe radiation frequencies from 3 to 30 kHz

Acknowledgements

Bibliography

Battan, L.J. 1965. Some factors governing precipitation and lightning from convective clouds. *J. Atmos. Sci.* **22**, 79–84

Bazelyan, E.M., Gorin, B.N., & Levitov, V.I. 1978. *Physical and Engineering Foundations of Lightning Protection*, 223 pp., Leningrad: Gidrometeoizdat

Berger, K., Anderson, R.B., & Kroninger, H. 1975. Parameters of lightning flashes. *Electra* **80**, 223–37

Betz, H.D., Schmidt, K., Laroche, P, Blanchet, P., Oettinger, W.P, Defer, E., Dziewit, Z., Konarski, J. 2009. LINET – An international lightning detection network in Europe. *Atmospheric Research* **91**, 564–573

Biagi, C.J., Cummins, K.L., Kehoe, K.E., & Krider, E.P. 2006. NLDN performance in Southern Arizona, Texas and Oklahoma in 2003–2004. *19th International Lightning Detection Conference*, Tucson, Arizona, USA

Boccippio, D.J., Williams, E.R., Heckman, S.J., Lyons, W.A., Baker, I.T., & Boldi, R. 1995. Sprites, ELF transients and positive ground strokes. *Science* **269**, 1088–91

Branick, M.L., & Doswell, C.A., III 1992: An observation of the relationship between supercell structure and lightning ground strike polarity. *Wea. Forecasting* **7**, 143–49

Brook, M., Nakano, M., Krehbiel, P., & Takeuti, T. 1982. The electrical structure of the Hokuriku winter thunderstorms. *J. Geophys. Res.* **87**, 1207–15

Browne, I.C. 1951. A radar echo from lightning. *Nature* **167**, 438

Carey, L.D., & Buffalo, K.M. 2007. Environmental control of cloud-to-ground lightning polarity in severe storms. *Mon. Weather Rev.* **135**, 1327–53

Carey, L.D., & Rutledge, S.A. 1996. A multiparameter radar case study of the microphysical and kinematic evolution of a lightning producing storm. *Meteor. Atmos. Phys.* **59**, 33–64

Carey, L.D., & Rutledge, S.A. 1998. Electrical and multiparameter radar observations of a severe hailstorm. *J. Geophys. Res.* **103**, 13 979–14 000

Carey, L.D., Rutledge, S.A., & Petersen, W.A. 2003. The relationship between severe storm reports and cloud-to-ground lightning polarity in the contiguous United States from 1989 to 1998. *Mon. Wea. Rev.* **131**, 121–1288

Carte, A. E., & Kidder, R.E. 1977. Lightning in relation to precipitation. *J. Atmos. Terr. Phys.* **39**, 139–48

Cerni, T.A. 1976. Experimental investigation of the radar cross section of cloud-to-ground lightning. *J. Appl. Meteor.* **15**, 795–8

Chalmers J.A. 1967 *Atmospheric electricity*, 2nd edition, Pergamon Press, New York

Changnon, S.A. 1992. Temporal and spatial relations between hail and lightning. *J. Appl. Meteorol.* **31**, 587–604

Chauveau B. 1925. *Electricité Atmospherique* (3 volumes), Libraire Octave Doin, Paris

Chauzy, S., Chong, M., Delannoy, A., & Despiau, S. 1985. The june 22 tropical squall line observed during Copt 81 experiment: Electrical signature associated with dynamical structure and precipitation. *J. Geophys. Res.* **90**, 6091–98

Chauzy, S., Coquillat, S., & Soula, S. 2005. On the relevance of Lightning Imagery from Geostationary Satellite Observation for Operational Meteorological Applications. UMR UPS/CNRS ordered by EUMETSAT

Chauzy, S. & Soula, S. 1999. Contribution of the ground corona ions to the convective charging mechanism. *Atmos. Res.* **51**, 179–300

Christian, H.J., Blakeslee, R.J., & Goodman, S.J. 1989. The detection of lightning from geostationary orbit. *J. Geophys. Res.* **94**, 13 329–37

Cianos, N., Oetzel, G.N., & Pierce, E.T. 1972. A technique for accurately locating lightning at close ranges. *J. Appl. Meteor.* **11**, 1120–7

Cramer, J.A., Cummins, K.L., Morris, A., Smith, R., & Turner, T.R. 2004. Recent Upgrades to the U.S. National Lightning Detection Network. *18th International Lightning Detection Conference*, Vaisala Inc., Helsinki, Finland

Cummins, K.L. 2000. Continental-scale detection of cloud-to-ground lightning. *Trans. IEE Japan* **120-B**, 2–5

Cummins, K.L., Murphy, M.J., Bardo, E.A., Hiscox, W.L., Pyle, R.B., & Pifer, A.E. 1998. A combined TOA/MDF technology upgrade of the US National Lightning Detection Network, *J. Geophys. Res.* **103**, 9035–9044

Ćurrić, M., & Vuković, Z.R. 1991. The influence of thunderstorm generated acoustic waves on coagulation: Part I. Mathematical formulation. *Z. Meteorol.* **41**, 164–169

Davis, M.H., Brook, M., Christian, H., Heikes, B.G., Orville, R.E., Park, C.G., Roble, R.G., & Vonnegut, B. 1983. Some scientific objectives of a satellite-borne lightning mapper. *Bull. Amer. Meteor. Soc.* **64**, 114–19

Delobbe, L., Crabbé, M., & Karim, H. 2004. Weather radar and lightning detection systems as complementary tools for hail thunderstorm detection. *18th International Lightning Detection Conference*

Doswell, C.A., II, & Brooks, H.E. 1993. Comments on 'Anomalous cloud-to-ground lightning in an F5-tornado-producing supercell thunderstorm on 28 August 1990.' *Bull. Amer. Meteor. Soc.* **74**, 2213–18

Dowden, R.L., Brundell, J.B., & Rodger, C.J. 2002. VLF lightning location by time of group arrival (TOGA) at multiple sites. *J. Atmos. Sol. Terr. Phys.* **64**, 817–830

Dwyer, J.R. 2003. A fundamental limit on electric fields in air. *Geophys. Res. Lett.* **30**, 2055, doi:10.1029/2003 GL017781

Eack, K.B., Beasley, W.B., Rust, W.D., Marshall, T.C., & Stolzenburg, M. 1996. X-ray pulses observed above a mesoscale convective system. *Geophys. Res. Lett.* **23**, 2915–18

Enell, C.F., Arnone, E., Adachi, T., Chanrion, O., Verronen, P.T., Seppälä, A., Neubert, T., Ulich, T., Turunen, E., Takahashi, Y., & Hsu, R.-R. 2008. Parameterisation of the chemical effect of sprites in the middle atmosphere. *Ann. Geophys.* **26**, 13–27

Eriksson, A.J. 1978. Lightning and tall structures. *Trans. S. Afr. IEE* **69**, 238–252

Ermakov, V.I., & Stozhkov, Y.I. 2003. Thunderclouds in the mechanism of solar-terrestrial-weather-climate relationship. *5th Russion conference on atmospheric electricity*

Fischer, H.J. 1977. Das luftelektrische feld in abhangigkeit von luftveruntreinigung und wetterlage, *Promotheus* **7/2**, 4–12

Fishman, G.J., Bhat, P.N., Mallozzi, R., Horack, J.M., Koshut, T., Kouveliotou, C., Pendleton, G.N., Meegan, C.A., Wilson, R.B., Paciesas, W.S., Goodman, S.J., & Christian, H.J. 1994. Discovery of intense gamma-ray flashes of atmospheric origin. *Science* **264**, 1313–16

Franklin, B. 1774. *Experiments and Observations of Electricity, Made at Philadelphia in America*, 5th edition, 530 pp., London: F. Newberry

Franz, R., Nemzek, R., Winckler, J. 1990. Television image of a large upward electrical discharge above a thunderstorm system. *Science* **249**, 48–51

Galarneau, T.J., Honikman, S.F., Cacciola, A.C., Bosart, L.F., LaPenta, K.D., Quinlan, J.S., & Wiley, G. 2000. Lightning in tornadic thunderstorms over the Northeastern United States. Preprints, *20th Conf. on severe local storms*, Orlando, FL, Amer. Meteor. Soc., 108–109

Gatlin, P.N., & Goodman, S.J. 2010. A total lightning trending algorithm to identify severe thunderstorms. *Journal of atmospheric and oceanic technology* **1**, 3–22

Gish, O.H., & Wait, G. R. 1950. Thunderstorms and the Earth's general electrification. *J. Geophys. Res.* **55**, 473–84

Goodman, S.J., Blakeslee, R., Christian, H., Koshak, W., Bailey, J., Hall, J., McCaul, E., Buechler, D., Darden, C., Burks, J., Bradshaw, T, & Gatlin, P. 2005. The North Alabama Lightning Mapping Array: Recent severe storm observations and future prospects. *Atmos. Res.* **76**, 423–37

Goyer, C.G. 1965a. Effects of lightning on hydrometeors. *Nature* **206**, 12203–09

Goyer, C.G. 1965b. Mechanical effects of a simulated lightning discharge on the water droplets of 'Old Faithful' Geyser. *Nature* **206**, 1302–1304

Gringel, W., Rosen, J.M., & Hoffman, D.J. 1986. Electrical structure from 0 to 30 km. In *The Earth's Electrical Environment*, eds. E.P. Krider, and R.G. Roble, pp. 166–82, Washington, DC: National Academy Press

Gurevich, A.V., Milikh, G.M., Roussel-Dupré, R.A. 1992. Runaway electron mechanism of air breakdown and preconditioning during a thunderstorm. *Phys. Lett. A.* **165**, 463–468

Harland, W.B., & Hacker, J.L.F. 1966. Fossil lightning strikes 250 million years ago. *Adv. Sci.* **22**, 663–671

Holle, R.L., & Lopez, R.E. 1993. Overview of real-time lightning detection systems and their meteorological uses. NOAA Techinal Memorandum ERL NSSL-102, 68 pp.

Holle, R.L., & Maier, M.W. 1982. Radar echo height related to cloud-ground lightning in south Florida. *12th Conf. on Severe Local Storms*, American Meteorological Society, 330–33

Holmes, C.R., Szymanski, E.W., Szymanski, S.J., & Moore, C.B. 1980. Radar and acoustic study of lightning. *J. Geophys. Res.* **85**, 7517–32

Idone, V.P., Davis, D.A., Moore, P.K., Wang, Y., Henderson, R.W., Ries, M., & Jamason, P.F. 1998a. Performance evaluation of the US National Lightning Detection Network in eastern New York, 1. Detection efficiency. *J. Geophys. Res.* **103**, 9045–55

Idone, V.P., Davis, D.A., Moore, P.K., Wang, Y., Henderson, R.W., Ries, M., & Jamason, P.F. 1998b. Performance evaluation of the US National Lightning Detection Network in eastern New York, 2. Location accuracy. *J. Geophys. Res.* **103**, 9057–69

Illingworth, A.J. 1985. Charge separation in thunderstorms: Small-scale processes. *J. Geophys. Res.* **90**, 6026–32

Inan, U.S., Barrington-Leigh, C., Hansen S., Glukhov, V.S., Bell, T.F., & Rairden, R. 1997. Rapid lateral expansion of optical luminosity in lightning induced ionospheric flashes referred to as 'elves'. *Geophys. Res. Lett.* **24**, 583–586

Jacobson, A.R., Cummins, K.L., Carter, M., Klinger, P., Roussel-Dupré, D., & Knox, S.O. 2000. FORTE radio-frequency observations of lightning strokes detected by the national Lightning Detection Network. *J. Geophys. Res.* **105**, 15 653–15 662

Jacobson, A.R., Holzworth, R., Harlin, J., Dowden, R., & Lay, E. 2006. Performance Assessment of the World Wide Lightning Location Network (WWLLN), using the Los Alamos Sferic Array (LASSA) as ground truth. *J. Atmos. and Oceanic Tech.* **23**, 1082–92

Jayaratne, E. R., Saunders, C.P.R., & Hallett, J. 1983. Laboratory studies of the charging of soft-hail during ice crystal interactions, *Q.J.R. Meteor. Soc.* **109**, 609–30

Jones, R.F. 1950. The temperature at the tops of radar echoes associated with various cloud systems. *Quart. J. Roy. Meteorol. Soc.* **76**, 312–30

Keogh, S.J., Hibbett, E., Nash, J., & Eyre, J. 2006. The Met Office Arrival Time Difference (ATD) system for thunderstorms detection and lightning location. *Forecasting Research Tech. Rep.* **488**, 22 pp.

Kidder, R.E. 1973. The location of lightning flashes at ranges less than 100 km. *J. Atmos. Terr. Phys.* **35**, 283–90

Kinzer, G.D. 1974. Cloud-to-ground lightning versus radar reflectivity in Oklahoma thunderstorms. *J. Atmos. Sci.* **31**, 787–99

Kuettner, J. 1950. The electrical and meteorological conditions inside thunderstorms. *J. Meteorol.* **7**, 322–32

Lagouvardos, K., Kotroni, V., Betz, H.-D., & Schmidt, K. 2009. A comparison of lightning data provided by ZEUS and LINET networks over Western Europe. *Nat. Hazards Earth Syst. Sci.* **9**, 1713–1717

Lang, T.J., & Rutledge, S.A. 2002, Relationships between convective storm kinematics, precipitation, and lightning. *Monthly Weather Review* **130**, 2492–2506

Lay, E.H., Holzworth, R.H., Rodger, C.J., Thomas, J.N., Pinto, O., & Dowden, R.L. 2004. WWLL Global Lightning Detection System: Regional Validation Study in Brazil. *Geophys. Res. lett.* **31**(3), L03102, 10.1029/2003GL018882

Lemonnier, L. G. 1752. Observations sur l'électricité de l'air. *Mem. Acad. Sci.* **2**, 223

Lhermitte, R., & Williams, E. 1985. Thunderstorm electrification: A case study. *J. Geophys. Res.* **90**, 6071–78

Ligda, M.G.H. 1950. Lightning detection with radar. *Bull. Amer. Meteor. Soc.* **31**, 279–83

Ligda, M.G.H. 1956. The radar observation of lightning. *J. Atmos. Terr. Phys.* **9**, 329–46

Liu, D., Feng, G., Wu, S. 2006. The characteristics of cloud-to-ground lightning activity in hailstorms over northern china. *Atmospheric Research* **91**, 459–465

Lojou, J.Y., Murphy, M.J., Holle, R.L., & Demetriades, N.W. 2008. Nowcasting of Thunderstorms Using VHF Measurements, in: "Lightning: Principles, Instruments and Applications", Eds. H.-D. Betz, U. Schumann, and P. Laroche, ch. 11, Dordrecht (NL), Springer, p. 253–270

Lopez, R.E., Ortiz, R., Otto, W.D., & Holle, R.E. 1990. The lightning activity and precipitation yield of convective cloud systems in central Florida. preprints, *25th International Conf. On Radar Meteorology*, Amer. Meteor. Soc. pp. 907–910

Lyons, W. 1994. Characteristics of luminous structures in the stratosphere above thunderstorms as imaged by low-light level video. *Geophys. Res. Lett.* **21**, 875–78

MacClement, W.D., & Murty, R.C. 1978. VHF direction finder studies of lightning. *J. Appl. Meteor.* **17**, 786–95

MacGorman, D.R., & Burgess, D.W. 1994. Positive cloud-to-ground lightning in tordanic storms and hailstorms. *Mon. Wea. Rev.* **122**, 1671–97

MacGorman, D.R., Burgess, D.W., Mazur, V., Rust, W.D., Taylor, W.L., & Johnson, B.C. 1989. Lightning rates relative to tornadic storm evolution on 22 May 1981. *J. Atmos. Sci.* **46**, 221–50

MacGorman, D.R., & Nielsen, K.E. 1991. Cloud-to-ground lightning in a tornadic storm on May 8 1996. *Mon. Wea. Rev.* **119**, 1557–74

MacGorman, D.R., & Rust, W.D. 1998. *The electrical nature of Storms*, Oxford University Press, 422 pp.

Mach, D.M., & Knupp, K.R. 1993. Radar reflectivity as a tool to remotely infer the presence of significant fields aloft. Preprints, *26th Intl. Conf. on Radar Meteorology*, Amer. Meteorol. Soc., 315–17

Maier, L., Lennon, C., Britt, T., & Schaefer, S. 1995. Lightning detection and ranging (LDAR) system performance and analysis. In *Sixth Conf. on Aviation Weather Systems*, Dallas, TX, Amer. Meteor. Soc., 305–309

Malan, D.J. 1952. Les Décharges dans l'air et la charge inférieure positive d'un nuage orageuse. *Ann.*

Geophys. **8**, 385–401

Marshall, T.C., & Rust, W.D. 1991. Electric field soundings through thunderstorms. *J. Geophys. Res.* **96**, 22 297–306

Marshall, T.C., Stolzenburg, M., Maggio, C.R., Coleman, L., Krehbiel, P., Hamlin, T., Thomas, R., & Rison, W. 2005. Observed Electric Fields Associated with Lightning Initiation. *Geophys. Res. Lett.* **32**, L03813

Marshall, T.C., & Winn, W.P. 1982. Measurements of charged precipitation in a New Mexico thunderstorm: Lower positive charge centers. *J. Geophys. Res.* **87**, 7141–57

Mazur, V. 1986. Rapidly occuring short duration discharges in thunderstorms, as indicators of a lightning-triggering mechanism. *Geophys. Res. Lett.* **13**, 355–58

McCarthy, M.P., Parks, G.K. 1985. Further observations of X-rays inside thunderstorms. *Geophys. Res. Lett.* **12**, 393–96

McCarthy, M.P., Parks, G.K. 1992. On the modulations of X-ray fluxes in thunderstorms. *J. Geophys. Res. Lett.* **97**, 5857–5864

McEachron, K.B. 1939. Lightning to the Empire State Building. *J. Franklin Inst.* **227**, 149–217

Michimoto, K. 1993. A study of radar echoes and their relation to lightning discharges of thunderclouds in the Hokuriku District. *J. Meteor. Soc. Jpn.* **71**, 195–204

Miller, S.L. 1953. Production of Amino Acids Under Possible Primitive Earth Conditions. *Science* **117**, 528–529

Montanyà, J., Pineda, N., March, V., Illa, A., Romero, D, & Solà, G. 2006. Experimental evaluation of the Catalan Lightning Detection Network. *19th International Lightning Detection Conference*, Tucson

Moore, C.B., Eack, K.B., Aulich, G.D., & Rison, W. 2001. Energetic radiation associated with lightning stepped leaders. *Geophys. Res. Lett.* **28**, 2141–2144

Moore, C.B., & Vonnegut, B. 1977. The thunder cloud. In: Golde, R.H. (Ed.), Lightning, Vol. 1. Academic, San Diego, USA, 51–98

Naccarato, K.P. 2005. Analysis of the cloud-to-ground lightning flashes characteristics in southeastern Brazil. PhD dissertation, Instituto Nacional de Pesquisas Espaciais (INPE)

Naccarato, K.P., & Pinto, O.Jr. 2008. The evolution of the detection efficiency model for the Brazilian lightning detection network (BrasilDAT). *20th International Lightning Detection Conference*, Tucson, Arizona, USA

Nickolaenko, A.P., Hayakawa, M. 2002, *Resonances in the Earth-Ionosphere Cavity*, Kluwer, Academic Publishers, Dordrecht

Oetzel, G.N., & Pierce, E.T. 1969. VHF technique for locating lightning. *Radio Sci.* **4**, 199–201

Ogawa, T. 1995. Lightning Currents. In *Handbook of Atmospheric Electrodynamics*, vol. I, ed. H. Volland, pp. 93–136, Boca Raton, FL: CRC Press

Orville, R.E. 1981. Global distribution of midnight lightning – September to November 1977. *Mon. Wea. Rev.* **109**, 391–5

Orville, R.E., 1991. Lightning ground flash density in the contiguous United States. *Mon. Wea. Rev.* **119**, 573–577

Orville, R.E., & Spenser, D.W. 1979. Global lightning flash frequency. *Mon. Wea. Rev.* **107**, 934–43

Orville, R.E., & Huffines, G.R. 2001, Cloud-to-ground lightning in the United States: NLDN results in the first decade, 1989–98, *Mon. Wea. Rev.* **129**, 1179–93

Orville, R.E., Huffines, G.R., Burrows, W.R., Holle, R.L., & Cummins, K.L. 2002. The North American Lightning Detection Network (NALDN)–first results: 1998–2000. *Mon. Weather. Rev.* **133**, 2098–2109

Perez, A.H., Wicker, L.J., & Orville, R.E. 1997. Characteristics of cloud-to-ground lightning associated with violent tornadoes. *Wea. Forecasting* **12**, 428–37

Pessi, A.T., Businger, S., Cummins, K.L., Demetriades, N.W.S., Murphy, M., & Pifer, B. 2009. *Journal of Atmospheric and Oceanic Tech.* **26**, 145–166

Piepgrass, M.V., Krider, E.P., & Moore, C.B. 1982. Lightning and surface rainfall during Florida thunderstorms. *J. Geophys. Res.* **87**, 11193–11201

Pineda, N., Bech, J., Rigo, T. & Trapero, L. 2006, Comparison of radar precipitation fields with lightning observations. *Proceedings of ERAD 2006*

Pinto, O. Jr, Naccarato, K.P., Pinto, I.R.C.A., Fernandes, W.A., & Pint Neto, O. 2006. Monthly distribution of cloud-to-ground lightning flashes as observed by lightning location systems. *Geophys. Res. Lett.* **33**, L09811, doi:10.1029/2006GL026081

Pinto, O. Jr, Pinto, I.R.C.A., Naccarato, K.P. 2007. Maximum cloud-to-ground lightning flash densities observed by lightning location systems in the tropical region: A review. *Atmospheric Research* **84**, 189–200

Pinto, O. Jr, Pinto, I.R.C.A. 2008. On the sensitivity of cloud-to-ground lightning activity to surface air tem-

perature changes at different time scales in the city of São Paulo, Brazil. *J. Geophys. Res.* **113**, D20123, doi:10.1029/2008JD009841

Raizer, Y.P. 1997. Gas Discharge Physics (Springer Verlag, New York)

Rakov, V.A. 2003. A review of positive and bipolar lightning discharges. *Bulletin of the American Meteorological Society* **84**, 767–776

Rakov, V.A., Uman, M.A. 2003. *Lightning, physics and effects*, Cambridge University Press, 687 pp.

Rakov, V.A., Uman, M.A., & Thottappillil, R. 1994. Review of lightning properties from electric field and TV observations. *J. Geophys. Res.* **99**, 10 745–50

Reap, R.M., & MacGorman, D.R. 1989. Cloud-to-ground lightning: climatological characteristics and relationships to model fields, radar observations, and severe local storms. *Mon. Weather Rev.* **117**, 518–35

Reid, G. C. 1986. Electrical structure of the middle atmosphere. In *The Earth's Electrical Environment*, eds. E.P. Krider, and R.G. Roble, pp.183–94, Washington, DC: National Academy Press

Rodger, C.J., Brundell, & Dowden, R.L. 2005. Location accuracy of long distance VLF lightning location network: post algorithm upgrade. *Ann. Geophys.* **23**(2), 277–290

Rodger, C.J., Werner, S.W., Brundell, J.B., Thomson, N.R., Lay, E.H., Holzworth, R.H., & Dowden, R.L. 2006. Detection efficiency of the VLF World-Wide Lightning Location Network (WWLLN): initial case study. *Annales Geophys.* **24**, 3197–3214

Rust, W.D., MacGorman, D.R., & Goodman, S.J. 1985. Unusual positive cloud-to-ground lightning in Oklahoma storms on 13 May 1983, *14th Conf. Severe Local Storms*, Indianapolis, AMS, pp. 372–75

Rust, W.D., Taylor, W.L., MacGorman, D.R., Brandes, E., Mazur, V., Arnold, R., Marshall, T., Christian, H., & Goodman, S.J. 1985. Lightning and related phenomena in isolated thunderstorms and squall line systems. *J. Aircraft* **22**, 449–54

Rutledge, S.A., Willima, E.R., & Keenan, T.D. 1992. The Down Under Doppler and Electricity Experiment (DUNDEE): Overview and preliminary results. *Bull. Am. Meteor. Soc.* **73**, 3–16

Schumann, W.O. 1952, Z. Naturforschung A **7**, 149–154

Schumann, W.O. 1957. Über die elektrische Eigenschwingungen des Hohlraumes Erde-Luft-Ionosphäre, erregt durch Blitzentladungen. *Z. Agnew. Phys.* **9**, 373

Schumann, W.O., & Koenig, H. 1954. Über die Beobachtung von Atmospherics bei geringsten Frequenzen. *Naturwissenschaften* **41**, 183–4

Sentman, D., & Wescott, E. 1993. Observations of upper atmospheric optical flashes recorded from an aircraft. *Geophys. Res. Lett.* **20**, 2857–2860

Sentman, D., Wescott, E., Osborne, D., Hampton, D., Heavner, M. 1995. Preliminary results from the Sprites94 Aircraft Campaign: 1. Red sprites. *Geophys. Res. Lett.* **22**, 1205–1208

Sentman, D., Stenbaek-Nielsen, H.C., McHarg, M.G., & Morrill., J.S. 2008. Plasma chemistry of sprite streamers. *J. Geophys. Res.* **113**, D11112, doi:10.1029/2007JD008941

Siingh, D., Gopalakrishnan, V., Singh, R. P., Kamra, A. K., Singh, S., Pant, V., Singh, R., & Singh, A. K. 2007, *Atmospheric Research* **84**, 91–110

Smith, D.A., Shao, X.M., Holden, D.N., Rhodes, C.T., Brook, M., Krehbiel, P.R., Stanley, M., Rison, W., & Thomas, R.J. 1999. A distinct class of isolated intracloud lightning discharges and their associated radio emissions. *J. Geophys. Res.* **104**, 4189–4212

Smith, D.M., Lopez, L.I., Lin, R.P., & Barrington-Leigh, C.P. 2005. Terrestrial Gamma-Ray Flashes Observed up to 20 MeV. *Science* **307**, 1085–1088

Soula, S., & Chauzy, S. 2001. Some aspects of the correlation between lightning and rain activities in thunderstorms. *Atmospheric Research* **56**, 355–73

Soula, S., Sauvageot, H., Molinié, G., Mesnard, F., & Chauzy, S. 1998. The CG lightning activity of a storm causing a flash-flood. *Geophys. Res. Lett.* **25**, 1181–84

Soula, S., Sauvageot, H., Saïssac, M. P., & Chauzy, S. 1995. Observation of thunderstorm by multilevel electric field measurement system and radar. *J. Geophys. Res.* **100**, 5025–35

Stolzenburg, M., Marshall, T.C., Rust, W.D. et al. 2007, Geophys. Res. Lett. **34**, L04804

Stozhkov, Y.I. 2003. The role of cosmic rays in the atmospheric processes. *Journal of Physics G.: Nuclear and Particle Physics* **29**, 913–23

Stozhkov, Y.I., Svirzhevsky, N.S., & Makhmutov, V.S. 2001. Cosmic ray measurements in the atmosphere, *preprint FIAN*, Moscow **8**, 1–25

Suszcynsky, D.M., Roussel-Dupré, R., & Shaw, G. 1996. Ground-based search for X-rays generated by thunderstorms and lightning. *J. Geophys. Res.* **101**, 23 505–16

Takahashi, T. 1978. Riming electrification as a charge generation mechanism in thunderstorms. *J. Atmos.*

Sci. **35**, 1536–48

Taylor, W.L. 1978. A VHF technique for space-time mapping of lightning discharge processes. *J. Geophys. Res.* **83**, 3575–83

Théry C. 2000. Evaluation of LPATS data using VHF interferometric observations of lightning flashes during the Eulinox experiment. *Eulinox experiment, final report*, Deutsches Zentrum für Luftund Raumfahrt, Oberpfaffenhofen, Germany

Thottappillil, R., Rakov, V.A., & Uman, M.A. 1990. K and M changes in close lightning ground flashes in Florida. *J. Geophys. Res.* **95**, 18 631–40

Turnman, B.N., & Edgar, B.C. 1982. Global lightning distributions at dawn and dusk. *J. Geophys. Res.* **87**, 1191–1206

Uman, M.A. 2001. *The lightning discharge,* Dover Publications Inc., New York

Uman, M.A., McLain, D.K., & Krider, E.P. 1975. The electromagnetic radiation from a finite antenna. *American Journal of Physics* **43**, 33–38

Vaughan Jr., O., Blakeslee, R., Boeck W., Vonnegut, B., Brook, M., & McKune, J. 1992. A cloud-to-space lightning as recorded by the Space Shuttle payload-bay TV camera. *Mon. Weather Rev.* **120**, 1459–1461

Vonnegut, B., & Moore, C.B. 1960. Possible effect of lightning discharge on precipitation formation process. *Geophys. Monogr.* **5**, 287–290

Waldvogel, A., Schmid, W., & Federer, B. 1978. Kinetic energy of hailfalls: part I. Hailstone spectra. *J. Appl. Meteorol.* **17**, 515–20

Wescott, E., Sentman, D, Heavner, M., Hampton, D, Osborne, D., Vaughan, Jr., O. 1996. Blue starters: Brief upward discharges from an intense Arkansas thunderstorm. *Geophys. Res. Lett.* **23**, 2153–2156

Williams, E.R. 1985. Large-scale charge separation in thunderclouds. *J. Geophys. Res.* **90**, 6013–25

Williams, E.R. 2001. The electrification of severe storms. *Meteorol. Monogr.* **28**, 527–61

Williams, E.R., Boldi, B., Matlin, A., Weber, M. Hodanish, S., Sharp, D., Goodman, S., Raghavan, R., & Buechler, D. 1999. The behavior of total lightning activity in severe Florida thunderstorms. *Atmos. Res.* **51**, 245–65

Williams, E.R., Mazur, V., & Geotis, S.G. 1990. Lightning investigation. In *Radar in Meteorology*, ed. D. Atlas, pp. 143–50, Boston, Massachusetts: Amer. Meteor. Soc.

Williams, E.R., Rutledge, S.A., Geotis, S.G., Renno, N., Rasmussen, E., & Rickenbach, T. 1992. A radar and electrical study of tropical "hot towers". *J. Atmos. Sci.* **49**, 1386–95

Williams, E.R., Zhang, R., & Rydock, J. 1991. Mixed-phase microphysics and cloud electrification. *J. Atmos. Sci.* **48**, 2195–2203

Wilson C.T.R. 1920. Investigations on lightning discharges and on the electric field of thunderstorms *Phil. Trans. Roy. Soc. Lond.* A 221, 73–115

Wilson C.T.R. 1929. Some thundercloud problems *J. Franklin Inst.* **208**, 1–12

Winn, W.P., Aldridge, T.V., & Moore, C.B. 1973. Video-tape recordings of lightning flashes. *J. Geophys. Res.* **78**, 4515–19

Workman, E.J., & Reynolds, S.E. 1949. Electrical activity as related to thunderstorm cell growth. *Bull. Am. Meteorol. Soc.* **30**, 142–44

Yair, Y., Israelevich, P, Devir, A.D., Moalem, M., Price, C., Joseph, J.H., Levin, Z., Ziv, B., Sternlieb, A., & Teller, A. 2004. New observations of sprites from the space shuttle. *J. Geophys. Res.* **109**, D15201, doi:10.1029/2003JD004497

Zajac, B.A., and J.F. Weaver, 2002: Lightning meteorology I: An introductory course on forecasting with lightning data. preprints, *Interactive Symp. on the Advanced Weather Interactive Processing System (AWIPS) and 18th International Conf. Interactive Information and Processing Systems (IIPS) for Meteorology, and Hydrology,* Orlando, Fl, Amer. Meteor. Soc., J8.6

Zipser, E.J. 1994. Deep cumulonimbus cloud systems in the tropics with and without lightning. *Mon. Wea. Rev.* **122**, 1837–51.

On the Science of Lightning:
An Overview
dr. Dieter R. Poelman